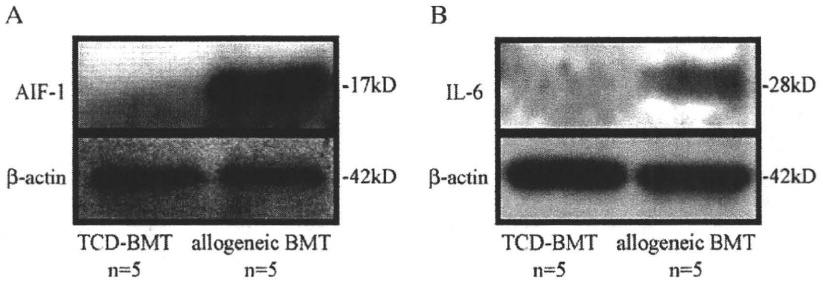

Fig. 3. Western blot analysis of AIF-1 and IL-6 in BMT skin tissues. Up-regulation of AIF-1 and IL-6 in skin tissues of Scl GVHD mice was detected compared with those of TCD-BMT mice by Western Blotting. (A) AIF expression, (B) IL-6 expression.

4. Discussion

In this study, we demonstrated that immunoreactive AIF-1 and IL-6 were significantly expressed in infiltrating mononuclear cells and fibroblasts in thickened skin of Scl GVHD mice compared with TCD-BMT mice. The immunohistochemical findings were confirmed by Western blot analysis. The effect of IL-6 production on NHDF by rAIF-1 was weak, despite which rAIF-1 increased the migration of NHDF directly. These findings suggest that AIF-1, which can induce the migration of fibroblasts and the production of IL-6 in affected skin tissues, is an important molecule promoting fibrosis in GVHD.

Allogeneic chronic GVHD presents with skin fibrosis like SSc [18]. Rapidly early cutaneous fibrosis which is one of the most critical pathological features in SSc is caused by the chemotactic migration of infiltrating mononuclear cells and fibroblasts [29]. In our study, AIF-1 was significantly expressed in infiltrating mononuclear cells and fibroblasts in thickened skin of Scl GVHD mice. AIF-1 was originally identified and cloned from rat cardiac allografts undergoing chronic rejection. To clarify the pathogenesis of GVHD it would be important to know how AIF-1 affects the migration and infiltration of those cells to target organs by chemotaxis. It has been recently shown that chemokine–chemokine receptor interactions such as CXCL12–CXCR4, CCL21–CCR7 induce the migration of fibrocytes or mesenchymal stem cells from bone marrow and play a role in the pathogenesis of tissue fibrosis [30,31]. There have been also many studies suggesting an association of bone marrow-derived cells with fibrosis [32,33]. These findings suggest that chronic fibroproliferative disorder is associated with various chemokines and chemokines affecting bone marrow-derived cells. So far, a relationship between AIF-1 and chemotaxis has been reported in some studies [14,34], but the AIF-1 was forcedly expressed by the stimulation of cytokines such as IFN-γ and TGF-β or by inserting the protein coding region of AIF-1 gene into cells [14,35]. We demonstrated that rAIF-1 itself has the function of chemotaxis in experiments with NHDF in a dose dependent manner. AIF-1 expressed in various tissues might be related to the pathogenesis of various immunoinflammatory diseases by the direct function of chemotaxis as we demonstrated.

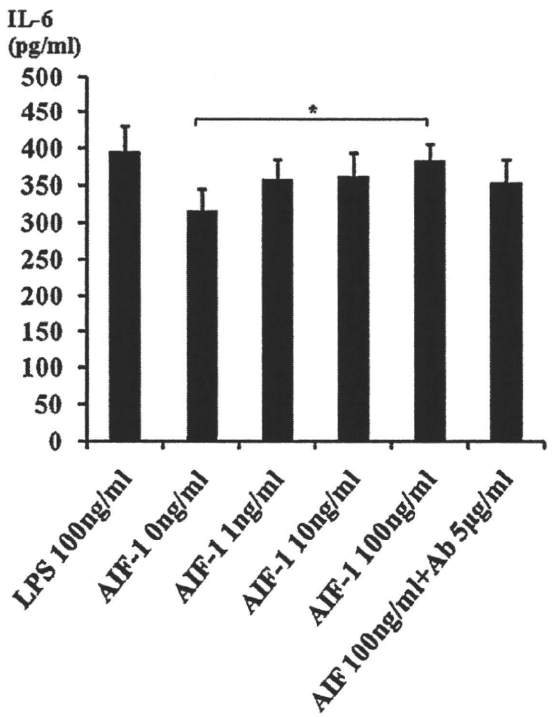

Fig. 4. IL-6 secretion from fibroblasts by rAIF-1. IL-6 concentration in the supernatant from cultured NHDF after rAIF-1 stimulation for 24 h. Each bar represents the mean ± SE of five experiments. The difference was analyzed by ANOVA followed by Bonferroni/Dunn's multiple comparison test. $^{*}p < 0.05$, $^{**}p < 0.01$.

IL-6 is a pleiotropic cytokine with multiple biological effects on immune regulation, haematopoiesis, inflammation, and oncogenesis, in addition to functioning as an autocrine or paracrine mediator on many cells [36]. We showed that rAIF-1 increased IL-6 production by synoviocytes, PBMCs [6]. In this study, IL-6 was also expressed in mononuclear cells and fibroblasts in the Scl GVHD model. Many reports have noted that PBMCs and fibroblasts of patients with SSc enhance induction of IL-6 [37] and that large amounts of serum IL-6 are strongly associated with the extent of skin and lung fibrosis in early SSc [38]. IL-6 induces increased production of collagen and glycosaminoglycans, hyaluronic acid and chondroitin-4/6-sulphates from human dermal fibroblasts [39]. Furthermore, IL-6 and TGF-β are inferred to lead to induction of IL-17 involved in the pathogenesis of SSc, because IL-17 induces inflammatory cytokines and cell adhesion molecules in fibroblasts, mononuclear cells, and endothelial cells [40,41]. AIF-1 may result in inducing cytokines and chemokines through secretion of IL-6, which leads to the migration of infiltrating inflammatory cells and fibroblasts.

We previously reported that rAIF-1 induces the proliferation of cultured synovial fibroblasts derived from RA in a dose-dependent manner [6]. It is also reported that AIF-1-transduced cells can enhance proliferation and can also promote entry into the cell cycle in the progression of the earliest phases (G1, G1/S transition) of the cell cycle, including cyclin E, cdks 6 and 7, and Skp1 [34]. In our inner preliminary study, skin dermal fibroblasts in primary culture from Scl GVHD mice did not show a significant migration and proliferation compared to those from control mice (data not shown). It is very difficult to demonstrate the function of dermal fibroblasts by use of primary culture in vitro because these cells were influenced by dealing with various reagents and conditions. However, the wound healing and WST-1 assays results that human rAIF-1 itself promoted the migration of dermal fibroblasts from human cell line but not the proliferation. These functions may be dependent on

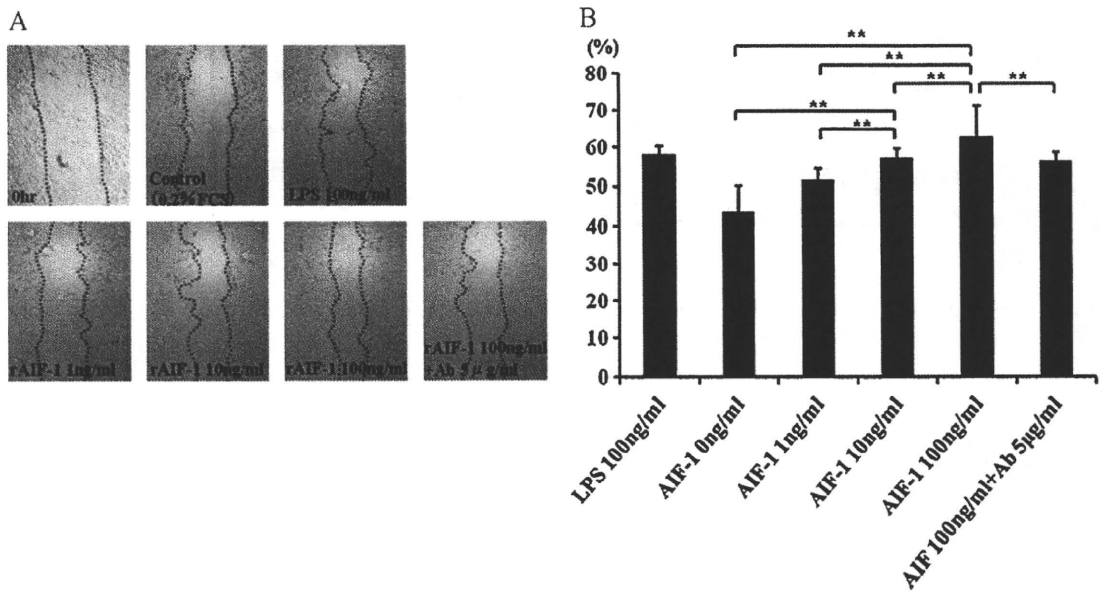

Fig. 5. AIF-1 increased NHDF migration. Scratch wounds of the confluent cell monolayer are cultured with or without AIF-1 or anti-AIF-1 Ab for 24 h. Each bar represents the mean ± SE of five experiments. Differences were analyzed by ANOVA followed by Bonferroni/Dunn's multiple comparison test. $^{**}p < 0.01$.

the types of cell and AIF. AIF protein we synthesized was named AIF-5 according to a new nomenclature of the AIF family of proteins [24]. This AIF splice variants IRT-1, G1, BART-1 are encoded in the same region of the BAT2 gene on chromosome 6 [5]. All variants contain a varying number of exons and transcripts. The modular architecture suggests that differential splicing mechanisms are responsible for the production of individual proteins. In addition, the migration was suppressed by adding anti-AIF-1 Ab as a neutralizing Ab. A receptor of AIF-1 has not been discovered yet and the mechanism of these actions will be further examined in the near future.

In conclusion, we suggest the possibility that AIF-1 may play an important role in the fibrosing process in Scl GVHD mice. The biological function of AIF-1 has not been completely elucidated, but it is sure that AIF-1 can induce IL-6 secretion on mononuclear cells and the chemotaxis of fibroblasts. AIF-1 may thus represent a new target for antifibrotic therapy in SSc as well as chronic GVHD. However, it is sure that not only fibroblasts but also macrophages, monocytes and lymphocytes produce IL-6 and various chemokines as factors inducing fibroblast activation and fibrosis. AIF-1 is thought to be one of these other responsible for fibroblast activation and fibrosis. The relationship between AIF-1 and these factors in the pathogenesis of GVHD needs to be pursued in the near future.

Acknowledgement

This study was supported by a Grant-in-Aid for Research (C) (No. 22591080) from The Ministry of Education, Culture, Sports, Science and Technology (MEXT) of Japan.

References

[1] Iris FJ, Bougueleret L, Prieur S, Caterina D, Primas G, Perrot V, et al. Dense Alu clustering and a potential new member of the NFB family within a 90 kilobase HLA class III segment. Nat Genet 1999;3:137–45.
[2] Autieri MV. cDNA cloning of human allograft inflammatory factor-1: tissues distribution, cytokine induction, and mRNA expression in injured rat carotid arteries. Biochem Biophys Res Commun 1996;228:329–76.
[3] Utans U, Arceci RJ, Yamashita Y, Russell ME. Cloning and characterization of allograft inflammatory factor-1: a novel macrophage factor identified in rat cardiac allografts with chronic rejection. J Clin Invest 1995;95:2954–62.
[4] Utans U, Quist WC, McManus BM, Wilson JE, Arceci RJ, Wallace AF, et al. Allograft inflammatory factor-1: a cytokine-responsive macrophage molecule expressed in transplanted human heart. Transplantation 1996;61:1387–92.
[5] Hara H, Ohta M, Ohta K, Nishimura M, Obayashi H, Adachi T. Isolation of two novel alternative splicing variants of allograft inflammatory factor-1. Biol Chem 1999;380:1333–6.
[6] Kimura M, Kawahito Y, Obayashi H, Ohta M, Hara H, Adachi T, et al. A critical role for allograft inflammatory factor-1 in the pathogenesis of rheumatoid arthritis. J Immunol 2007;178:3316–22.
[7] Del Galdo F, Maul GG, Jimenez SA, Artlett CM. Expression of allograft inflammatory factor 1 in tissues from patients with systemic sclerosis and in vitro differential expression of its isoforms in response to transforming growth factor-β. Arthritis Rheum 2006;54:2616–25.
[8] Otieno FG, Lopez AM, Jimenez SA, Gentiletti J, Artlett CM. Allograft inflammatory factor-1 and tumor necrosis factor single nucleotide polymorphisms in systemic sclerosis. Tissue Antigens 2007;69:583–91.
[9] Pawlik A, Kurzawski M, Szczepanik T, Dziedziejko V, Safranow K, Borowiec-Chłopek Z, et al. Association of allograft inflammatory factor-1 gene polymorphism with rheumatoid arthritis. Tissue Antigens 2008;72:171–5.
[10] Alkassab F, Gourh P, Tan FK, McNearney T, Fischbach M, Ahn C, et al. An allograft inflammatory factor 1 (AIF1) single nucleotide polymorphism (SNP) is associated with anticentromere antibody positive systemic sclerosis. Rheumatology (Oxford) 2007;46:1248–51.
[11] Takehara K. Pathogenesis of systemic sclerosis. J Rheumatol 2003;30:755–9.
[12] Duncan MR, Frazier KS, Abramson S, Williams S, Klapper H, Huang X, et al. Connective tissue growth factor mediates transforming growth factor beta-induced collagen synthesis: down-regulation by cAMP. FASEB J 1999;13:1774–86.
[13] Igarashi A, Nashiro K, Kikuchi K, Sato S, Ihn H, Grotendorst GR, et al. Significant correlation between connective tissue growth factor gene expression and skin sclerosis in tissue sections from patients with systemic sclerosis. J Invest Dermatol 1995;105:280–4.
[14] Kelemen SE, Autieri MV. Expression of allograft inflammatory factor-1 in T lymphocytes: a role in T-lymphocyte activation and proliferative arteriopathies. Am J Pathol 2005;167:619–26.
[15] Del Galdo F, Jiménez SA. T cells expressing allograft inflammatory factor 1 display increased chemotaxis and induce a profibrotic phenotype in normal fibroblasts in vitro. Arthritis Rheum 2007;56:3478–88.
[16] Orsmark C, Skoog T, Jeskanen L, Kere J, Saarialho-Kere U. Expression of allograft inflammatory factor-1 in inflammatory skin disorders. Acta Derm Venereol 2007;87:223–7.
[17] Tian Y, Jain S, Kelemen SE, Autieri MV. AIF-1 expression regulates endothelial cell activation, signal transduction, and vasculogenesis. Am J Physiol Cell Physiol 2009;296:256–66.
[18] Furst DE, Clements PJ, Graze P, Gale R, Roberts N. A syndrome resembling progressive systemic sclerosis after bone marrow transplantation. A model for scleroderma? Arthritis Rheum 1979;22:904–10.
[19] Zhang Y, McCormick LL, Desai SR, Wu C, Gilliam AC. Murine sclerodermatous graft-versus-host disease, a model for human scleroderma: cutaneous cytokines, chemokines, and immune cell activation. J Immunol 2002;168:3088–98.
[20] Rogai V, Lories RJ, Guiducci S, Luyten FP, Matucci-Cerinic M. Animal models in systemic sclerosis. Clin Exp Rheumatol 2002;26:941–6.
[21] McCormick LL, Zhang Y, Tootell E, Gilliam AC. Anti-TGF-beta treatment prevents skin and lung fibrosis in murine sclerodermatous graft-versus-host disease: a model for human scleroderma. J Immunol 1999;163:5693–9.
[22] Nagira T, Matthew SB, Yamakoshi Y, Tsuchiya T. Enhancement of gap junctional intercellular communication of normal human dermal fibroblasts cultured

on polystyrene dishes grafted with poly-N-isopropylacrylamide. Tissue Eng 2005;11:1392–7.
[23] Kawata E, Ashihara E, Kimura S, Takenaka K, Sato K, Tanaka R, et al. Administration of PLK-1 small interfering RNA with atelocollagen prevents the growth of liver metastases of lung cancer. Mol Cancer Ther 2008;7:2904–12.
[24] Deininger MH, Meyermann R, Schluesener HJ. The allograft inflammatory factor-1 family of proteins. FEBS Lett 2002;514:115–21.
[25] Yamada R, Sano H, Hla T, Hashiramoto A, Fukui W, Miyazaki S, et al. Auranofin inhibits interleukin-1β-induced transcript of cyclooxygenase-2 on cultured human synoviocytes. Eur J Pharmacol 1999;385:71–9.
[26] Furuya M, Kato H, Nishimura N, Ishiwata I, Ikeda H, Ito R, et al. Down-regulation of CD9 in human ovarian carcinoma cell might contribute to peritoneal dissemination: morphologic alteration and reduced expression of beta1 integrin subsets. Cancer Res 2006;5:2617–25.
[27] Kikuchi Y, Takai T, Ota M, Kato T, Takeda K, Mitsuishi K, et al. Application of immunoreaction enhancer solutions to an enzyme-linked immunosorbent assay for antigen-specific IgE in mice immunized with recombinant major mite allergens or ovalbumin. Int Arch Allergy Immunol 2006;141:322–30.
[28] Uchida H, Maruyama T, Ono M, Ohta K, Kajitani T, Masuda H, et al. Histone deacetylase inhibitors stimulate cell migration in human endometrial adenocarcinoma cells through up-regulation of glycodelin. Endocrinology 2007;148:896–902.
[29] Distler JH, Akhmetshina A, Schett G, Distler O. Monocyte chemoattractant proteins in the pathogenesis of systemic sclerosis. Rheumatology 2009;48:98–103.
[30] Mehrad B, Burdick MD, Strieter RM. Fibrocyte CXCR4 regulation as a therapeutic target in pulmonary fibrosis. Int J Biochem Cell Biol 2009;41:1708–18.
[31] Lama VN, Phan SH. The extrapulmonary origin of fibroblasts: stem/progenitor cells and beyond. Proc Am Thorac Soc 2006;3:373–6.
[32] Lin WR, Brittan M, Alison MR. The role of bone marrow-derived cells in fibrosis. Cells Tissues Organs 2008;188:178–88.
[33] Strieter RM, Gomperts BN, Keane MP. The role of CXC chemokines in pulmonary fibrosis. J Clin Invest 2007;117:549–56.
[34] Chen X, Kelemen SE, Autieri MV. AIF-1 expression modulates proliferation of human vascular smooth muscle cells by autocrine expression of G-CSF. Arterioscler Thromb Vasc Biol 2004;24:1217–22.
[35] Autieri MV, Carbone C. Expression of allograft inflammatory factor-1 is a marker of activated human vascular smooth muscle cells and arterial injury. Arterioscler Thromb Vasc Biol 2000;20:1737–44.
[36] Kishimoto T. The biology of interleukin-6. Blood 1989;74:1–10.
[37] Feghali CA, Bost KL, Boulware DW, Levy LS. Mechanisms of pathogenesis in scleroderma I. Overproduction of interleukin 6 by fibroblasts cultured from affected skin sites of patients with scleroderma. J Rheumatol 1992;19:1207–11.
[38] Hasegawa M, Sato S, Fujimoto M, Ihn H, Kikuchi K, Takehara K. Serum levels of interleukin 6 (IL-6), oncostatin M, soluble IL-6 receptor, and soluble gp130 in patients with systemic sclerosis. J Rheumatol 1998;25:308–13.
[39] Duncan MR, Berman B. Stimulation of collagen and glycosaminoglycan production in cultured human adult dermal fibroblasts by recombinant human interleukin 6. J Invest Dermatol 1991;97:686–92.
[40] Kurasawa K, Hirose K, Sano H, Endo H, Shinkai H, Nawata Y, et al. Increased interleukin-17 production in patients with systemic sclerosis. Arthritis Rheum 2000;43:2455–63.
[41] Murata M, Fujimoto M, Matsushita T, Hamaguchi Y, Hasegawa M, Takehara K, et al. Clinical association of serum interleukin-17 levels in systemic sclerosis: is systemic sclerosis a Th17 disease? J Dermatol Sci 2008;50:240–2.

Available online at www.sciencedirect.com

ScienceDirect

ELSEVIER

Nanomedicine: Nanotechnology, Biology, and Medicine xx (2011) xxx–xxx

nanomedicine

www.nanomedjournal.com

Original Article

Single-step, label-free quantification of antibody in human serum for clinical applications based on localized surface plasmon resonance

Junta Yamamichi, MS, MPH[a,b], Tetsunori Ojima, MS[a], Kimiko Yurugi[c], Mie Iida, MS[a], Takeshi Imamura, MS[a], Eishi Ashihara, MD, PhD[c], Shinya Kimura, MD, PhD[c,d,*], Taira Maekawa, MD, PhD[c]

[a]*High Performance Sensing Research Division, Frontier Research Center, Canon Inc., Tokyo, Japan*
[b]*Department of Biostatistics, Boston University School of Public Health, Boston, Massachusetts*
[c]*Department of Transfusion Medicine and Cell Therapy, Kyoto University Hospital, Kyoto, Japan*
[d]*Division of Hematology, Respiratory Medicine and Oncology, Department of Internal Medicine, Faculty of Medicine, Saga University, Saga, Japan*

Received 24 August 2010; accepted 1 February 2011

Abstract

The amount of antibody in blood is an important measure of health status for making critical decisions in clinical practice. Here, we demonstrated a single-step, label-free, molecular diagnositic method based on localized surface plasmon resonance (LSPR) using standard 96-well microtiter plates. We improved the LSPR biosensor so that it can measure antibodies to blood group antigens in human serum with a single-step operation. First, we employed the ampholytic polymeric surface modification technique to present an efficient molecular scaffold on the sensor surface. Second, we selected the combination of an appropriate reference molecule against the antigen and a blocking agent to significantly reduce the variability of signal due to nonspecific responses of the unknown in the sample. Finally, we overcame the analytical difficulty arising from serum and achieved a single-step "wash-free" measurement of the amount of target antibody in human serum.

Key words: Optical biosensor; Localized surface plasmon resonance; Immunoassay; Blood test

In clinical tests, antibody titers in blood are very important measures for diagnosis. Antibodies related to infectious diseases such as chickenpox or hepatitis are among the conventional targets of those tests. In autoimmune diseases such as rheumatoid arthritis or systemic lupus erythematosus, autoantibodies play an important role in diagnosis as well. Other examples like blood group ABO-related immunoglobulin levels after living-donor organ transplantations are critically essential for treatments and prognosis of transplantees because antibody-mediated rejection is one of the primary causes of poor outcomes.[1] Several methods are used to measure antibody levels in serum. They include enzyme-linked immunosorbent assay (ELISA), radioimmunoassay (RIA), and fluorescence-activated flow cytometry (FACS). Moreover, among the various new types of chemical and biological sensors, the optical method using surface plasmon resonance (SPR) on planar gold films has made a particularly important contribution to affinity-based biosensing applications, including antigen-antibody reactions, during the past two decades. As mentioned in the reviews,[2-4] the SPR sensor has been widely used to monitor the change in the refractive index induced by a broad range of analyte bindings in a label-free manner. This direct detection method of biomolecules eliminates conventional signal transducers such as fluorophore and enzyme.

In our previous work,[5,6] we showed that the SPR method could be used to measure anti-human blood group A (anti-A) IgG titers in sera rapidly and quantitatively while avoiding the interference from IgM-type antibodies. This could be a promising tool because one of the clinical interests is the amount of IgG-type antibodies. Measurement of anti-A IgG titers in sera has been routinely conducted by the conventional test tube (TT) method. This method, however, has the intrinsic problem of interexaminer variability because it relies on visual observation.[7] Our study was the initial trial for clinical use of the SPR method. It improved the diagnostic operation by intermittently

The authors declare no conflict of interest.

*Corresponding author.
E-mail address: shkimu@cc.saga-u.ac.jp (S. Kimura).

1549-9634/$ – see front matter © 2011 Elsevier Inc. All rights reserved.
doi:10.1016/j.nano.2011.02.002

monitoring the level of the same patients' antibodies after clinical ABO-unmatched transplant.

However, because the SPR method is based on flow-cell type sensor chips, the resultant sequential operation is very complex and a more efficient procedure is desired in clinical practice. This instrumental characteristic possibly limits the reduction of the total assay time and the achievement of a high-throughput assay system. In addition, the SPR method detects unknown species, not only in the vicinity of the sensing planar gold surface, but at a relatively long distance from its surface. This can cause unpredictable and unnecessary responses of signals that affect the accuracy of the measurement and mandate the temperature control of the whole system to minimize the fluctuation of the refractive index. Therefore, signal compensations such as a reference flow cell or subsequent washing are necessary. Moreover, it requires us to regenerate a sensor chip surface before another test is to be done. It is quite a complex process to prepare the new sensor chip surface with the same sensor characteristics as previous ones. From the analytical viewpoint, these properties are not favorable to control the quality of each measurement in the long run.

In this article, inspired by the similarity to the SPR method and its less practical applicability, we further explore the possibility of the application of the localized surface plasmon resonance (LSPR) method[8] to this kind of measurement. As one of the promising technologies to acquire the information of molecular binding events, this method can be made with very simple set-up and assay procedures in comparison with those of SPR. Through the advance of nanofabrication techniques and nanophotonics, this particular label-free immunoassay has been widely investigated for many biological applications.[9-14] Previously, we have demonstrated its simple fabrication in a 96-well microtiter plate format and its applicability to a label-free immunoassay with the expectation that this method can be used in clinical tests.[15] We have found the density of immobilized gold nanoparticles (AuNPs) best to detect antibody in sample solution.

When metal nanoparticles are excited by light, their conduction electrons on the surface, known as surface plasmons, exhibit collective oscillations. These oscillations result in both absorption and scattering of incident light of a specific resonant wavelength. This phenomenon is called LSPR. The characteristic resonance energy of the surface plasmon is strongly dependent on the dielectric properties of the local environment around the nanometric particles.[16,17] Thus, small changes in the refractive index induced by surrounding liquid or analyte binding at or near the surface of nanometric particles can be measured as shifts in the LSPR spectra. We believe that the LSPR method has the benefits of both SPR and ELISA. These include a label-free simple assay like SPR and a high-throughput parallel operation like ELISA.

To our knowledge, our investigation is the first clinical application of the LSPR method with human blood samples. We measured anti-A IgG levels in human serum based on LSPR to compare with the previously established methods by SPR. Our study focused on simplicity, reproducibility and accuracy with respect to the clinical diagnosis. One of the difficulties in the label-free methodology is reducing the nonspecific responses from serum to increase the intensity of specific response. For this purpose, we employed novel zwitterionic copolymer to serve as a molecular scaffold on the surface of AuNPs. It can adsorb strongly onto the gold surface with static ionic interaction between its amino groups and gold and present efficient grafting points for further chemical modification on the surface of NPs, such as immobilization of antigen groups or blocking agents through its carboxyl groups, which would eventually lead to the improvement of signal intensity. Due to the improved signal intensity, the final measurements can be done even without removing and washing the serum before the measurements. We call this the "wash-free" measurement that simplifies the process as a single-step assay of a specific analyte in serum. Putting the test solution into a reaction well could be the only required operation to achieve accurate diagnostic results. Finally, for validation of our method, comparison of the results with several other diagnostic methods was also performed.

Methods

Functionalization of the surface of AuNPs

Ninety six-well polystyrene amine surface microtiter plates (Corning, Corning, New York) were used as the substrates on which the AuNPs (100 nmφ; BBInternational, Cardiff, United Kingdom) were immobilized at the optimized density.[15] The surface of AuNPs were functionalized with polyampholite polymer PAS-410 (Nitto Boseki, Fukushima, Japan) and human blood group A trisaccharide antigen molecules (Carbohydrate Synthesis, Oxford, United Kingdom). Details in preventing nonspecific adsorption are described in the Supporting Information.

LSPR measurement of the levels of target antibody (anti-A)

Serum samples were taken from 41 healthy adult volunteers at Kyoto University Hospital, including 21 men and 20 women with informed consents according to the Declaration of Helsinki. Crude human serum was diluted by one third, using a diluent containing 0.26% PAS-410 and 0.01% BSA in phosphate buffered saline (PBS) (pH 7.0) to prepare the test solution. Without dilution, some samples were within the range of saturation of signal. Therefore, we decided to dilute all crude samples in this work. The diluent consisted of components similar to those on the surface of AuNPs, and we aimed to avoid unnecessary interaction between the sample and sensor surface. A 100 μL aliquot of the test solution was then incubated for 30 minutes at room temperature (24–25°C). Next, we measured its optical extinction spectrum in the "wash-free" condition. Subsequently, each well was washed and filled with 100 μL PBS. The optical extinction spectrum was measured again in the "wash" condition. The specific peak shift induced by the antibodies bound to immobilized antigens was obtained by subtracting the peak shift of the reference-well measured at the same point in time. With the purified anti-A IgG diluted in PBS, we created a plot of concentration-dependent shift of spectrum peak (λ_{max}) to estimate concentrations of the antibodies in the test solution. In addition, a

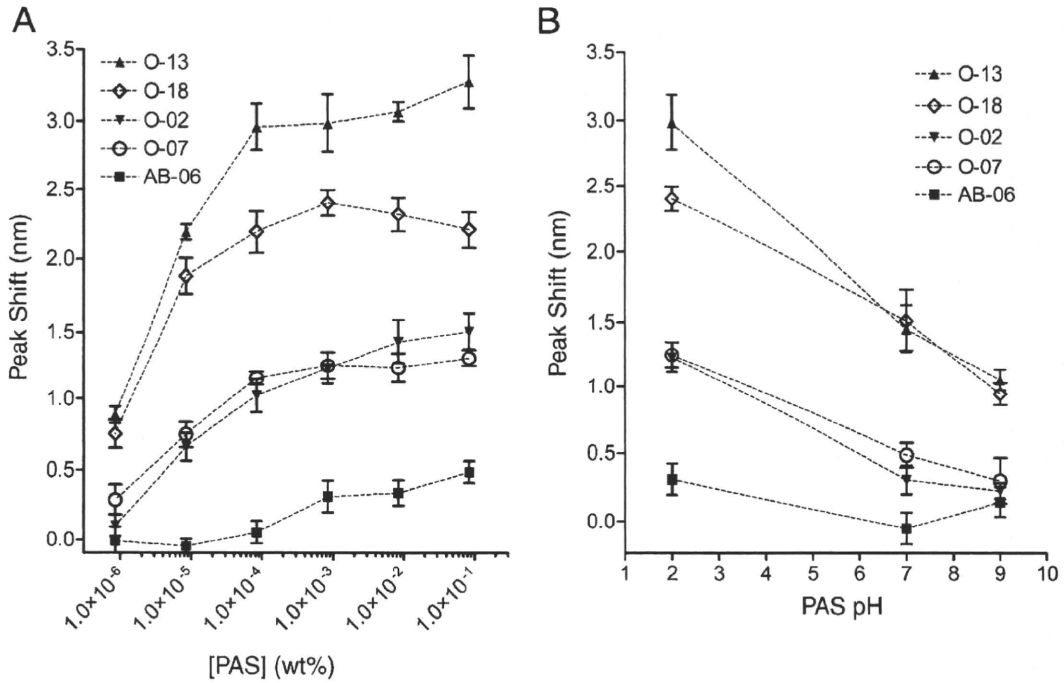

Figure 1. Effect of coating polymer concentrations and pH levels on sensor responses (spectrum peak (λ_{max}) shift). **(A)** Effect of concentration. **(B)** Effect of pH level. Data was acquired using the sera from 4 blood group O and 1 blood group AB volunteers. Error bars represent standard errors.

secondary analysis was performed to quantify bound IgG-type antibodies by adding a 100 μL aliquot of 100 μg/mL goat anti-human IgG monoclonal antibody (Rockland Immunochemicals, Gilbertsville, Pennsylvania) and incubating for 30 minutes at 37°C. The final spectra measurement was performed after being completely dried with compressed dried air. A plate reader (Varioskan; Thermo Fisher Scientific, Waltham, Massachusetts) was used to measure the optical extinction spectra of immobilized AuNPs on the plates. The spectra data were analyzed by fitting them to a Gaussian curve to identify a spectrum peak (IGOR Pro; WaveMetrics, Portland, Oregon).

Determination of antibody levels by the TT and SPR method and their correlation with those measured by the LSPR method

We employed the same procedure described elsewhere for the TT and SPR measurements.[5,6] For the SPR method, we used Biacore X system (GE Healthcare, Amersham, United Kingdom). The blood group A trisaccharide antigen molecules were immobilized on the sensor chip CM5 following the standard procedures. An anti-human IgG monoclonal antibody (Sanbio, Uden, The Netherlands) diluted with the running buffer HBS-EP (GE Healthcare) was used to measure the amounts of anti-A IgG associated with the blood group antigen A immobilized on the chip. All measurements were performed at 25°C. The deviations among different sensor chips were adjusted using the responses from the identical serum sample. We performed a statistical evaluation of correlation of the results from 3 methods. We computed linear correlations of both the TT and SPR methods with the LSPR method (SAS 9.1 software; SAS Institute, Cary, North Carolina).

Results

Sensor functionalization and assay optimization

Our sensor elements consisted of monodisperse AuNPs, which were immobilized on the surface of polystyrene microtiter plates as reported in our previous work.[15] Microtiter plates are very useful for multiplexing the assay on the same plate. Fundamentally, our LSPR method is characterized by determining shifts of λ_{max}, which are the measure of changes in the refractive index at or near the proximity of the surface of AuNPs. These shifts are induced by specific analyte binding to target elements on the surface of AuNPs and are to be converted into the actual amount of analyte molecules bound on the surface using the standard response curve. Spectrum measurement was done by standard plate reader. The surface of AuNPs was first coated with the polyampholytic polymer anchored on their surface by its amino groups. The polymer is a novel water-soluble zwitterionic copolymer composed of diallylamine hydrochloride salt and maleic acid. This polymer provides us with efficient grafting points for the target element of human blood group A trisaccharide antigen through its carboxyl groups. The characteristics of the polyampholytic polymer are strongly affected by pH levels, which in turn change the sensor properties. Thus, at first we evaluated the sensing properties in terms of signal intensity with various pH levels and concentrations of the polymer solution to achieve good selectivity (Figure 1). We used 5 representative human sera for this optimization, including 4 blood group O and 1 blood group AB. Although the variation of the concentration of anti-A in serum is relatively large even in healthy volunteers, it may due to the difference in individual exposure to the antigen. The serum of blood group AB works as a negative control

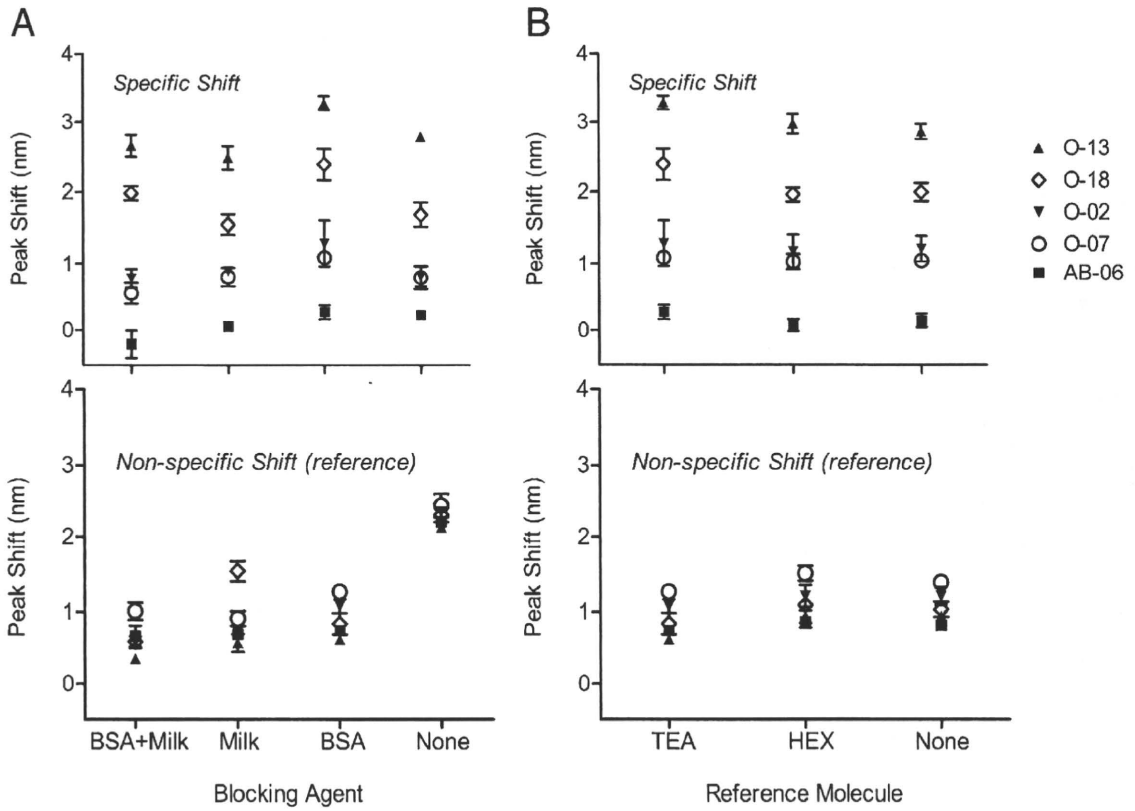

Figure 2. Comparison of effects of blocking agents and reference molecules on sensor responses (shift of λ_{max}). **(A)** Effect of blocking agents: BSA+Skim milk, Skim milk, BSA and None. **(B)** Effect of reference molecules: TEA, HEX and None. The upper graphs represent data from signal wells, whereas the lower graphs represent data from reference wells. Data were acquired using the sera from 4 blood group O and 1 blood group AB volunteers. Error bars represent standard errors.

because we do not expect any response to the blood group A antigen from the serum of blood group AB. We chose the optimum condition for coating as 8.4×10^{-4} % (w/w) at pH 2.0 hereafter, which was in the middle of the stable condition having a large response.

In the second step of the optimization, we further investigated the selection of blocking agents and reference molecules, which would reduce the unknown signals from crude samples and enable a single-step, label-free measurement. We tried well-known blocking agents of BSA, skim milk and their combination. For reference molecules, which were immobilized on the surface of AuNPs in the reference well, we tried TEA and HEX. Based on the result shown in Figure 2, we conclude that choosing BSA and TEA for blocking agent and reference molecule, respectively, can achieve larger signal. Then, we were convinced that the optimum condition of our assay had been achieved and we were ready to proceed to measure various serum samples. Again, we observed a good selectivity towards anti-A antibody also in this optimized condition by using serum of blood group AB.

Validation: Concentration-dependent shifts of λ_{max} by purified human anti-A antibody

We confirmed concentration-dependent shifts of λ_{max} as basic characteristics of our LSPR sensor using purified target antibody: human anti-A antibody (Figure 3). We fitted this profile assuming a 1:1 binding model between anti-A and blood group A antigen. The fitted curve provides us the dissociation constant (K_d) of 1.5×10^{-4} g/mL. Due to the difficulty of preparing a higher concentration of purified anti-A antibody from human blood, we did not measure λ_{max} in a higher concentration range than 40 μg/mL. However, with using the serum that has the highest concentration of anti-A antibody, we observed the similar trend of shifts of λ_{max} across our experimental concentration range.

Challenge: single-step, wash-free measurement of serum samples

We applied our assay to the various samples from volunteers and investigated the applicability of a single-step measurement in crude samples. The difference between the process of "wash" and "wash-free" measurement concerns whether we replace the serum in each well with a buffer solution before performing the spectrum measurement. In the single-step "wash-free" measurement, we do not discard the serum and we proceed directly to the spectrum measurement. The major purpose of this "wash" operation is to significantly reduce the signal from the unknown species in the serum and improve the accuracy of the measurement. Figure 4 compares the signals from both operations. Interestingly, the slope of linear regression between 2 methods is identical to unity with $R^2 = 0.91$. This means that there is no significant difference between them. We therefore conclude that the single-step "wash-free" measurement works

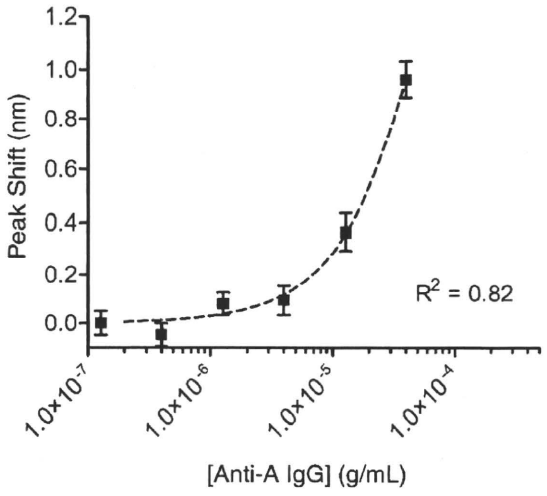

Figure 3. Anti-A concentration-dependent shifts of λ_{max}. Dotted line shows a sigmoidal fitting to the experimental data. Error bars represent standard errors from 8 samples.

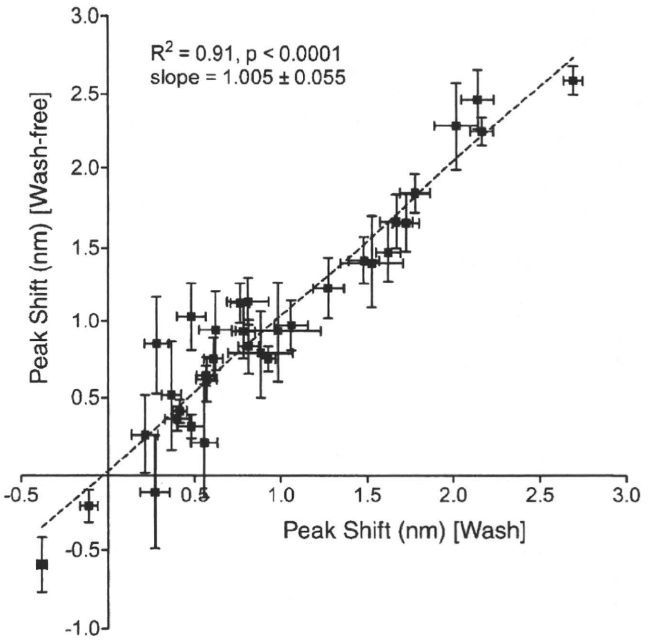

Figure 4. Wash-free measurement. Correlation between "wash-free" and "wash" measurements. Dotted line was determined by linear regression analysis (slope = 1.005, R^2 = 0.91). Error bars represent standard errors.

equivalently to the standard "wash" operation without any significant interference from the serum in the well.

Comparison of the single-step assay with other methods

Finally, we compared our single-step "wash-free" assay with other methods, i.e., TT and SPR, using the common 41 serum samples (Figure 5, *A*). Because two major isotypes of antibodies exist in serum, i.e., IgG and IgM-types, we conducted a supplemental measurement using the secondary antibody (anti-human IgG) that specifically detects the amount of IgG-type anti-A antibody bound on the AuNPs and computed the correlations separately in those two types of measurements (Table 1). As for the TT method, the procedure we used for the computation of correlations is generally assumed to measure IgG-type antibody only. We observed at least moderately strong correlations among the methods. For the IgG-type antibody, the correlation coefficient between LSPR and TT is smaller than that observed between LSPR and SPR (0.66 vs. 0.79). This is possibly due to the less quantitative nature of the TT method, in which results are discrete values. For instance, the TT results of many samples were zero in Figure 5, *B*. On the other hand, correlation coefficients between LSPR and SPR are approximately 0.8 (strong) for both types of measurement, and more than 60% of the variability in the LSPR results is explained statistically by SPR (Figure 5, *A*). In particular, we did not find a difference in the correlations between the measurements of total antibody and IgG-type in the comparison of LSPR and SPR. Thus, we conclude that LSPR and SPR measured the similar types of antibody in our assay because two types of measurements (i.e., total and IgG-type antibody) did not change the correlation between the two methods.

Discussion

Development of a rapid, accurate and sensitive diagnostic method is favored in clinical practices from both financial and ethical points of view. With this goal, many types of new biosensors have been proposed and presented to the clinical community for use in diagnostics. Meanwhile, TT and ELISA have been widely used along with accumulated empirical evidence and increased confidence, even though they require sophisticated operations and substantial time to complete. We believe that one of the tipping points where the clinical community will accept a new method depends on the extent of its simplicity of operation and reproducibility of results relative to the conventional methods.

In this study, we demonstrated a more efficient approach to quantify the amount of antibodies in sera while fulfilling practical requirements. We optimized our assay to detect antibodies in both nano-optical[15] and surface chemical aspects as shown in Figures 1 and 2. The optimal arrangement of immobilized AuNPs and the use of a polyampholytic polymer are two essential elements of our method. The former enhanced the sensitivity and the latter enabled efficient surface chemistry and high selectivity. Though the zwitterionic copolymer looks difficult to control in a stable manner, we found its optimum condition to facilitate surface modification. We believe that larger signal responses using the acidic polymer solution are caused by the dense attachment of the polymer on the surface of AuNPs due to static attraction between positively charged polymer chains and negatively charged AuNPs. The capability of blocking nonspecific binding is similar for BSA and skim milk (Figure 2), but we cannot expect a synergetic effect using both materials simultaneously. From our experience, BSA seems to be a more stable agent for long-term storage. To optimize a reference well, we tried 2 kinds of molecules (i.e., TEA and HEX). As expected, slightly better trends were achieved using more hydrophilic molecules, which have a relatively similar

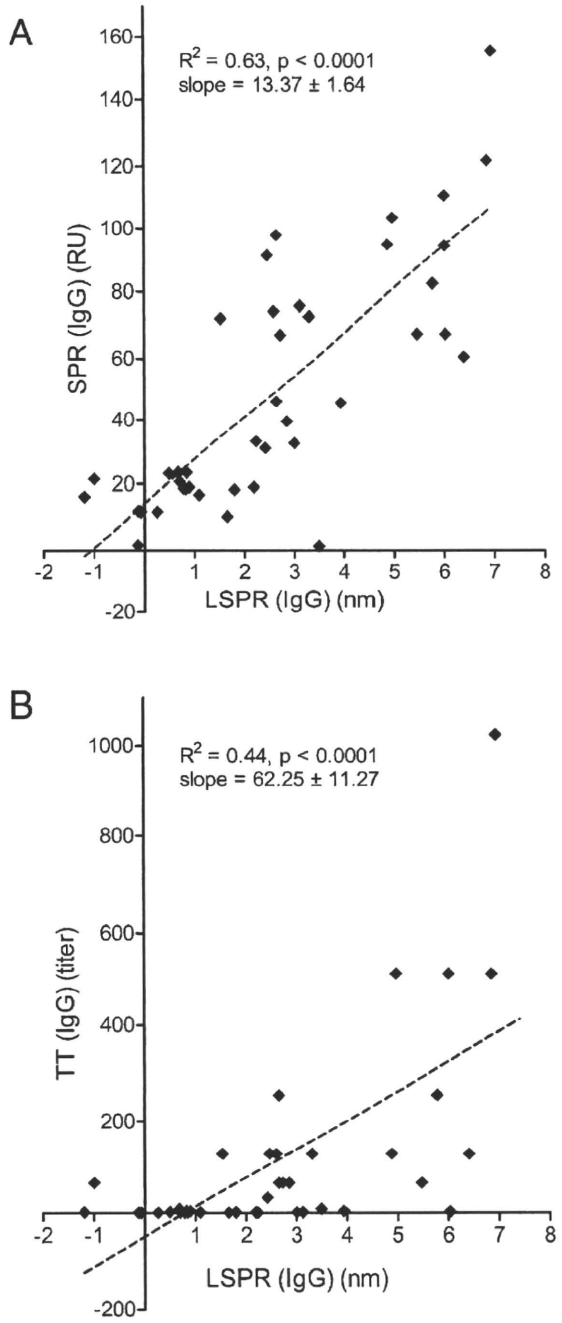

Figure 5. Correlations between TT, SPR and LSPR measurements of 41 volunteers. **(A)** Between SPR (IgG) and LSPR (IgG). Dotted line was determined by linear regression analysis (slope = 13.37, R^2 = 0.63). **(B)** Between TT (IgG) and LSPR (IgG). Dotted line was determined by linear regression analysis (slope = 62.25, R^2 = 0.44).

molecular characteristic to the trisaccharide antigen. Attained sensitivity and selectivity both contributed to the success of single-step "wash-free" measurement. A calibration plot of λ_{max} as a function of anti-A antibody concentration shows a detection limit of <10 μg/mL (Figure 3). This plot is based on the specific shift subtracted by nonspecific shift. Thus, a lower bound of error bar should simply exceed zero at the detection limit. Using a streptavidin-biotin reaction in diluted human blood, Wang et al

Table 1
Pearson correlation coefficients between assays

	TT (IgG)	SPR (Total)	SPR (IgG)
LSPR (Total)	0.70	0.80	0.78
LSPR (IgG)	0.66	0.80	0.79

The correlation coefficients were computed with the data from the common 41serum samples.

obtained a detection limit of about 3 μg/mL.[13] We are convinced that our results are within a reasonable range using an antigen-antibody reaction.

In comparison with other methods, we observed at least moderately strong correlations among them (Table 1). A statistical interpretation of R-squares is that at most, 44% and 63% of variability of the results in LSPR were to be explained by TT and SPR, respectively (Figure 5). In other words, we should be cautious about considering other factors that influence the measurements. This is because such methods do not necessarily measure exactly the same events that LSPR measures. Particularly, TT is less quantitative, for which results are discrete values based on serial dilutions and visual observation. Moreover, SPR uses a flow-cell system, which means it detects a dynamic process of binding events, not a static process. These diferences would contribute to the decreased correlations or R–squares.

It is well known that human serum has several isotypes of antibody dominated by IgG and IgM, which was confirmed by the TT method here. We consider it in the case of our assay. We suppose that LSPR and SPR detect mostly the IgG-type antibody, which we presume from their similar responses even without the use of the secondary antibody. That secondary antibody was used to distinguish IgG and IgM. This is, to some extent, due to the higher K_d of IgM antibodies in a monovalent intereraction[18] between antigen-binding region and immobilized antigen than that of IgG. In our assay by LSPR or SPR, IgG and IgM competed against each other for the same targeting antigen. Our observation of results, however, is that the major responses are caused by the reaction of IgG, owing to its higher affinity to the antigen than IgM. Therefore, we conclude that LSPR could substitute for the function of SPR in measuring antibody titers and improve the operability in clinical practice because of their similar diagnostic characteristics in terms of the isotypes of antibody to be measured.

Two features of our method are worth mentioning with respect to the clinical diagnostics. First, our assay is simple, and a single-step operation is possible. Figure 4 reveals the equivalency of responses between "wash" and "wash-free" measurements. The near-zero intercept also indicates the competence of our technique to prevent nonspecific adsorption from serum contents. This is owing to the spatial characteristic of the LSPR biosensor as illustrated in the Graphical Abstract. Specifically, LSPR has a smaller sensing volume than SPR, which is appropriate to exclusively detect the surface binding events. In addition, we have optimized the sensing volume for detecting antibodies as reported previously.[15] We emphasize this property because none of the conventional methods is able to measure quantitatively with a single step. This observation would bring a huge benefit in clinical practice because the only required

procedure to get accurate diagnostic results is to put the test solution into a reaction well. This means a substantial reduction of total operational time to measure the concentration of antibodies. In addition, it could eliminate other laborious manual steps like washing wells, which can cause deviation in the responses obtained by many laboratory technicians in clinical practice. Furthermore, intermittent monitoring of specific markers in the sample could be easily conducted in a clinical setting using our method because the quality of each measurement well can be precisely controlled. For example, monitoring the change in the amount of anti-human blood group antigen antibodies is essential for prognosis after the ABO-unmatched transplant. The risk of adverse events in the case of ABO-incompatible living-liver transplantation would decrease significantly with timely monitoring and appropriate remedies. With the help of our methods, physicians will have better opportunities to more accurately follow up on patients' critical responses to the transplants than in the past.

Second, as our assay used microtiter plates, we are easily able to multiplex the measurement because the required sample is small and the operation is simple. In many situations, physicians are interested in a set of different antibodies or biomolecules to improve the performance of diagnosis of a patient's condition. For instance, multiplexed markers for autoimmune diseases or tumors are used and explored.[19-22]

Further intensive study is necessary to improve this assay. A major drawback to our demonstrated method is the use of reference wells, which is also a fundamental challenge in the development of label-free optical biosensors. This duplicates the operation to improve signal intensity. However, we hope to find a way to obtain accurate results even without reference wells. Moreover, this single-well measurement will provide a real-time measurement of molecular binding events, which enables us to understand the affinity and kinetics of that binding event similarly by the SPR method.

In conclusion, we have shown a single-step, label-free quantification of anti-A antibodies in human serum. Our method achieved a simple, efficient and reliable way to specifically detect antibodies in crude serum samples. These results point to the vast applicability of our LSPR method to measure the level of antibodies in the test solution by adopting various kinds of antigens immobilized on AuNPs. We believe that the LSPR method will have the potential to be routinely used as a rapid and cost-effective diagnostic method in the future.

Appendix A. Supplementary data

Supplementary data to this article can be found online at doi:10.1016/j.nano.2011.02.002.

References

1. Egawa H, Teramukai S, Haga H, Tanabe M, Fukushima M, Shimazu M. Present status of ABO-Incompatible living donor liver transplantation in Japan. Hepatology 2008;47:143-52.
2. Homola J, Yee SS, Gauglitz G. Surface plasmon resonance sensors: review. Sens Actuators B: Chem 2000;63:24-30.
3. Englebienne P, Van Hoonacker A, Verhas M. Surface plasmon resonance: principles, methods and applications in biomedical sciences. Spectrosc 2003;17:255-73.
4. Campbell CT, Kim G. SPR microscopy and its applications to high-throughput analyses of biomolecular binding events and their kinetics. Biomater 2007;28:2380-92.
5. Kimura S, Yurugi K, Segawa H, Kuroda J, Sato K, Nogawa M, et al. Rapid quantitation of immunoglobulin G antibodies specific for blood group antigens A and B by surface plasmon resonance. Transfusion 2005;45:56-62.
6. Yurugi K, Kimura S, Ashihara E, Tsuji H, Kawata A, Kamitsuji Y, et al. Rapid and accurate measurement of anti-A/B IgG antibody in ABO-unmatched living donor liver transplantation by surface plasmon resonance. Transfusion Med 2007;17:97-106.
7. Kobayashi T. Standardization of the assay method for anti-A/B antibody titers and its problems. Int Congress Series 2006;1292:3-7.
8. Anker JN, Hall WP, Lyandres O, Shah NC, Zhao J, Van Duyne RP, et al. Biosensing with plasmonic nanosensors. Nat Mater 2008; 7:442-53.
9. Nath N, Chilkoti AA. Colorimetric Gold nanoparticle sensor to interrogate biomolecular interactions in real time on a surface. Anal Chem 2002;74:504-9.
10. Englebienne P. Use of colloidal gold surface plasmon resonance peak shift to infer affinity constants from the interactions between protein antigens and antibodies specific for single or multiple epitopes. Analyst 1998;123:1599-603.
11. Haes AJ, Chang L, Klein WL, Van Duyne RP. Detection of a biomarker for Alzheimer's disease from synthetic and clinical samples using a nanoscale optical biosensor. J Am Chem Soc 2005;127:2264-71.
12. Mayer KM, Lee S, Liao H, Rostro BC, Fuentes A, Scully PT, et al. A label-free immunoassay based upon localized surface plasmon resonance of gold nanorods. ACS Nano 2008;2:687-92.
13. Wang Y, Qian W, Tan Y, Ding S. A label-free biosensor based on gold nanoshell monolayers for monitoring biomolecular interactions in diluted whole blood. Biosens Bioelectron 2008;23:1166-70.
14. Endo T, Kerman K, Nagatani N, Takamura Y, Tamiya E. Label-free detection of peptide nucleic acid-DNA hybridization using localized surface plasmon resonance based optical biosensor. Anal Chem 2005;77:6976-84.
15. Yamamichi J, Iida M, Ojima T, Handa Y, Yamada T, Kuroda R, et al. The mesoscopic effect on label-free biosensors based on localized surface plasmon resonance of immobilized colloidal gold. Sens Actuators B: Chem 2009;143:349-56.
16. Kelly KL, Coronado E, Zhao LL, Schatz GC. The optical properties of metal nanoparticles: the influence of size, shape, and dielectric environment. J Phys Chem B 2003;107:668-77.
17. Miller MM, Lazarides AA. Sensitivity of metal nanoparticle plasmon resonance band position to the dielectric environment as observed in scattering. J Opt A: Pure Appl Opt 2006;8:S239-49.
18. Strandh M, Ohlin M, Borrebaeck CAK, Ohlson S. New approach to steroid separation based on a low affinity IgM antibody. J Immunol Methods 1998;214:73-9.
19. Döner T, Hansen A. Autoantibodies in normals - the value of predicting rheumatoid arthritis. Arthritis Res Ther 2004;6:282-4.
20. Hanly JG, Thompson K, McCurdy G, Fougere L, Theriault C, Wilton K. Measurement of autoantibodies using multiplex methodology in patients with systemic lupus erythematosus. J Immunol Methods 2010;352: 147-52.
21. Binder S. Autoantibody Detection Using Multiplex Technologies. Lupus 2006;15:412-21.
22. Vojdani A. Antibodies as predictors of complex autoimmune diseases and cancer. Int J Immunopathol Pharmacol 2008;21:553-66.

ANTICANCER RESEARCH *30*: 245-252 (2010)

Absence of Oncogenic Mutations of *RAS* Family Genes in Soft Tissue Sarcomas of 100 Japanese Patients

YONGHUI JIN[1], YASUKO SHIMA[1,2], MORITOSHI FURU[1,2], TOMOKI AOYAMA[2,3], TAKEHARU NAKAMATA[2], TOMITAKA NAKAYAMA[2], TAKASHI NAKAMURA[2] and JUNYA TOGUCHIDA[1,2,4]

[1]*Department of Tissue Regeneration, Institute for Frontier Medical Sciences;*
[2]*Department of Orthopaedic Surgery and* [3]*Human Health Sciences, Graduate School of Medicine, and*
[4]*Center for iPS Research and Application, Institute of Integrated Cell-Material Science,*
Kyoto University, Kyoto, Japan

Abstract. *Background: Activating point mutations of genes of the RAS family (KRAS, HRAS and NRAS genes) are frequently found in carcinomas, but their prevalence in sarcomas varies considerably among ethnic groups. No extensive studies in Japanese patients have been performed. Materials and Methods: Mutation analyses of three RAS genes (KRAS, HRAS and NRAS) were performed using polymerase chain reaction-single strand conformation polymorphism (PCR-SSCP) analyses and PCR direct sequencing in one hundred cases of soft tissue sarcoma (STS) as well as six STS cell lines from Japanese patients. Results: No mutations were found in two hot spot regions (codon 12-13 and 61) of the three RAS genes. Conclusion: Activating mutations of the RAS gene family are uncommon events in soft tissue sarcomas in Japanese patients.*

The detection of oncogene mutations in tumors has not only led to a better understanding of tumorigenesis, but also aided in diagnosis and treatment. *RAS* genes are the most frequently found activating oncogenes in human carcinomas. They gain their oncogenic activity *via* a single amino acid substitution in codon 12, 13 or 61 of the *KRAS*-, *HRAS*- or *NRAS*-encoded p21 protein (1). Point mutations occurring in *RAS* genes give rise to proteins with reduced intrinsic GTPase activity associated with oncogenesis (2). Some reports have indicated that *RAS* oncogenes have no ability to transform primary cells and mutant Ras proteins can only transform cells that have undergone predisposing changes such as immortalization (3, 4). We have previously reported that an activated *HRAS* gene transformed mesenchymal stem cells only when they were immortalized beforehand by the introduction of a human telomerase catalytic subunit (*hTERT*) and *BMI1* gene (5).

Activated *RAS* genes have frequently been found in adenocarcinomas of the pancreas (90%), colon (50%), thyroid (50%) and lung (30%) (6). Soft tissue sarcomas (STSs) account for fewer than 1% of human malignancies and fewer than 2% of cancer deaths (7, 8). They present a heterogeneous group of tumors with respect to origin and morphological features. Previous studies have provided inconsistent results, with the frequency of *RAS* mutations in STS ranging from 0% to 44% (9-17). The inconsistency may be due to small sample numbers, incomplete sensitivity of the detection methods or the patients' ethnic origin. Moreover, no reports have investigated all codons 12, 13 and 61 of *KRAS, HRAS* and *NRAS* genes in a large number of samples.

In the present study, extensive analyses in codons 12, 13 and 61 of the *KRAS, HRAS* and *NRAS* genes were performed in one hundred STS samples and six STS cell lines from Japanese patients. To increase sensitivity, two methods were used to detect mutations: polymerase chain reaction-single strand conformation polymorphism (PCR-SSCP) and PCR direct sequencing.

Materials and Methods

Tissue specimens and cell lines. Tumor tissues were obtained from 100 patients with STS tumors, which were obtained at either biopsy or resection in Kyoto University Hospital. The Ethics Committee of the Faculty of Medicine, Kyoto University, approved the procedure and informed consent was obtained from each donor. There were 60 female and 40 male patients and their median age was 52.5 years (10 to 90). The pathological diagnoses are described in Table I. Histological analyses were performed in all the samples, which showed that more than 90% of each tissue was composed of tumor cells.

Six STS cell lines derived from Japanese patients were also analyzed in this study (Table I). YaFuSS (synovial sarcoma) was established in our laboratory (18). HS-SY-II (synovial sarcoma) was a gift from H. Sonobe (Kochi Medical School, Japan) (19), SYO-1

Correspondence to: J. Toguchida, Institute for Frontier Medical Sciences, Kyoto University, 53 Kawahara-cho, Shogoin, Sakyo-ku, Kyoto 606-8507, Japan. Tel: +81 757514134, Fax: +81 757514646, e-mail: togjun@frontier.kyoto-u.ac.jp

Key Words: RAS, mutation, soft tissue sarcoma, Japan.

Table I. *Pathological diagnoses of STS patients and STS cell lines.*

Diagnoses	No. of tumor tissues	No. of cell lines
Liposarcoma	20	0
well-differentiated	2	
myxoid	12	
pleomorphic	4	
dedifferentiated	2	
MFH	14	0
Synovial sarcoma	10	4
Leiomyosarcoma	11	0
MPNST	9	1
ARMS	5	1
Solitary fibrous tumor	4	0
Epitheliod sarcoma	3	0
Fibrosarcoma	2	0
Myxofibrosarcoma	2	0
ASPS	2	0
Clear cell sarcoma	2	0
PNET	1	0
DFSP	1	0
Malignant hemangiopericytoma	1	0
UDS	13	0
	100	6

MFH, malignant fibrous histiocytoma; MPNST, malignant peripheral nerve sheath tumors; ARMS, alveolar rhabdomyosarcoma; ASPS, alveolar soft part sarcoma; PNET, primitive neuroectodermal tumor; DFSP, dermatofibrosarcoma protuberans; UDS, undifferentiated sarcoma.

Table II. *Point mutations in positive control cell lines.*

Gene	DNA sequences at target codons			Cell line with each mutation	
	12	13	61	Name	Tumor type
Wild-type					
KRAS	GGT	GGC	CAA		
HRAS	GGC	GGT	CAG		
NRAS	GGT	GGT	CAA		
Mutant					
KRAS	G**T**T	GGC	CAA	SW480	colon carcinoma
KRAS	GGT	GGC	CA**T**	PR310 *	lung carcinoma
HRAS	G**T**C	GGT	CAG	EJ	bladder carcinoma
HRAS	GGC	GGT	C**T**G	SK-2 *	melanoma
NRAS	G**A**T	GGT	CAA	MOLT-4	leukemia
NRAS	GGT	GGT	**A**AA	HT1080	fibrosarcoma

*Plasmids containing mutant fragments were used to replace cell lines.

(synovial sarcoma) was from A. Kawai (Okayama University, Japan) (20), Fuji (synovial sarcoma) was from S. Tanaka (Hokkaido University, Japan) (21), NMS-2 (malignant peripheral nerve sheath tumor) was from A. Ogose (Niigata University, Japan) (22), and KP-RMS-DM (alveolar rhabdomyosarcoma) was from H. Hosoi (Kyoto Prefectural University of Medicine, Japan) (23). For the positive controls in mutation analyses, cell lines known to have oncogenic *RAS* gene mutations were used: HT1080 (fibrosarcoma), SW480 (colon carcinoma), EJ (bladder carcinoma) and MOLT-4 (leukemia), all of which were purchased from the American Type Culture Collection (ATCC) (Manassas, VA, USA).

DNA extraction. High molecular weight DNA was isolated from the tumor tissues and cell lines by standard phenol-chloroform extraction methods (24).

Positive and negative controls for analyses. For the positive control in the PCR-SSCP analyses, PCR fragments containing specific mutations were amplified using cell lines with each mutation (25) (Table II). Because no cell lines containing mutations in codon 61 of the *KRAS* and *HRAS* genes were available, mutant fragments were created according to the literature (25) for each mutation: Codon 61 of the *KRAS* gene in PR310 (lung carcinoma) and codon 61 of the *HRAS* in SK-2 (melanoma). Briefly, corresponding PCR fragments of the *KRAS* and *HRAS* genes were amplified from primary human skin fibroblasts, and cloned into pCR2.1 vector (Invitrogen, Carlsbad, CA, USA). Each mutation was introduced into the fragment by site-directed mutagenesis using a PrimeSTAR Mutagenesis Basal Kit (TAKARA Bio Inc, Otsu, Japan). The plasmids containing each mutant fragment for *KRAS* and *HRAS* were designated Mut-PR310 and Mut-SK-2, respectively and used as template DNA for the PCR-SSCP analyses.

PCR-SSCP analysis. The prevalence of the *RAS* mutations in the 100 STS samples and cell lines was investigated by PCR-SSCP, as previously described (26, 27). A previous study had shown 97% of mutations to be detected in 100- to 300-base-long strands (28). Genomic DNA (200 ng) was amplified using 20 pmol of sense and antisense primers (Table III) in a 50 μl reaction mixture with a final $MgCl_2$ concentration of 1.5 or 2.0 mM using AmpliTaq Gold DNA Polymerase (Applied Biosystems, Foster City, CA, USA). All the PCR programs included an initial denaturation for 5 min at 94°C, followed by 35 cycles of 30 sec at 94°C, 30 sec at the annealing temperature (Tm) for each PCR primer pair and 1 min at 72°C, with a final extension at 72°C for 7 min. The PCR products were electrophoresed through a 2.0% agarose gel with ethidium bromide to confirm the quality of amplification. Aliquots of the reaction mixtures denatured at 95°C for 5 min in a dilution buffer (0.1% SDS and 10 mM EDTA) were loaded onto a 15% polyacrylamide gel (acrylamide/bisacrylamide 19:1) with 10% glycerol and run for 3 to 4 h at 30 W and 10°C. The bands were visualized with a DNA Silver Staining Kit (Bio-Rad, Richmond, CA, USA).

Direct DNA sequencing. Six sets of PCR primers were designed to cover the entire coding region of the *RAS* gene and small introns (Table III). In each PCR, 200 ng of genomic DNA was used as a template and amplification was performed in a 50 μl reaction mixture with 20 pmol of each primer, 1 unit of AmpliTaq Gold DNA Polymerase and 1.5 mM $MgCl_2$, using GeneAmp PCR System 9700 (Applied Biosystems). The efficiency of the reaction was confirmed based on an analysis of the products by electrophoresis in a 1.5% agarose gel. The products were then purified using the QIAquik PCR purification kit (Qiagen, Tokyo, Japan). The purified PCR products were sequenced with a BigDye Terminator v3.1 cycle sequencing kit (Applied Biosystems) on an automated DNA

Table III. *Primers used for the PCR-SSCP and direct sequencing.*

Gene	Target codon	Primers for PCR-SSCP			Primers for direct sequencing		
		Name	Sequence	Length of amplified fragment (bp)	Name	Sequence	Length of amplified fragment (bp)
KRAS	12-13	K1a	ACTGAATATAAACTTGTGGTAGTTGGAGCT	135	K1-SF	TGGAGGAGTTTGTAAATGAAG	533
		K1b	TAATATGCATATTAAAACAAGATTTACCTC		K1-SR	ACCCTGACATACTCCCAAG	
KRAS	61	K2a	TTCCTACAGGAAGCAAGTAG	128	K2-SF	CTATTGATGATGTTGAGCATC	514
		K2b	CACAAAGAAAGCCCTCCCCA		K2-SR	ATAAAACAGGGATATTACCTAC	
HRAS	12-13	H1a	AGGAGACCCTGTAGGAGGACC	126	H1-SF	GGCACGCTGCAGTCCTTG	587
		H1b	TGGTTCTGGATCAGCTGGATG		H1-SR	CCTGCTTCCGGTAGGAATC	
HRAS	61	H2a	TCCTGCAGGATTCCTACCGG	194	H2-SF	CGAATACGACCCCACTATAG	649
		H2b	GGTTCACCTGTACTGGTGGA		H2-SR	CGAGTCCTTCACCCGTTTG	
NRAS	12-13	N1a	GACTGAGTACAAACTGGTGG	118	N1-SF	GTGTGAGGCCGATATTAATC	446
		N1b	GGGCCTCACCTCTATGGTG		N1-SR	TGTTCTCTATAAACACGTTAAG	
NRAS	61	N2a	GGTGAAACCTGTTTGTTGGA	103	N2-SF	TTAGCAATTTGAGGGACAAAC	557
		N2b	ATACACAGAGGAAGCCTTCG		N2-SR	CAAGCTTCACTTATGTATTATC	

sequencer (3130/3130xl Genetic Analyzer, Applied Biosystems). A DNA sequence analysis was performed with 3130/3130xl Genetic Analyzer Data Collection Software v3.0 (Applied Biosystems).

Results

PCR-SSCP analyses. To confirm the quality of the PCR-SSCP analyses, fragments encompassing either codons 12-13 or codon 61 of each *KRAS, HRAS* and *NRAS* gene were amplified from the cell lines listed in Table II as well as the normal fibroblasts and electrophoresed on non-denaturing gel. The plasmids containing a mutant fragment (pMut-PR310 or pMut-SK-2) were also used as a DNA template for the positive control. Clear mobility shifted bands were detected in all cases (Figure 1A). Contamination from normal cells in tumor tissues may cause false negative results. To investigate the sensitivity of our PCR-SSCP method, DNA was extracted from mixtures of cells with each mutation and normal fibroblasts and analyzed. In the case of mutations in codons 12-13 of *HRAS*, clear mobility shifted-bands were detected if the fraction of tumor cells (EJ) made up more than 10% of all the cells (Figure 1B). Similar results were obtained in the other regions (data not shown), proving the quality and sensitivity of the PCR-SSCP method used in this study.

PCR-SSCP was then performed using DNA samples from the surgical specimens of STSs and the cell lines. The results of five samples in six regions are shown in Figure 2. The positive control samples showed clear mobility-shifted bands in each region, whereas no such shifted bands were detected in the STS samples. None of the 100 samples and six cell lines showed mobility shifted-bands in any of the six regions.

Direct sequencing. To confirm the results of PCR-SSCP analyses, each target region was analyzed by direct sequencing. Figure 3 shows the results for six regions in one STS sample. Positive control samples derived from either cell lines or plasmids showed the expected point mutations as previously described, whereas only the normal sequence was found in the sarcoma samples. No mutation was detected in these 6 regions of the 100 STS samples and six STS cell lines.

Discussion

STSs are defined as malignant tumors arising in mesenchymal tissues except bone and cartilage, and have a wide variety of types. There are several ways to classify STSs, for example, based on morphology (small round cell or spindle cell), grade of differentiation (well- or poorly-differentiated), or grade of malignant phenotype (high, intermediate, or low grade malignancy). In terms of molecular genetics, STSs can be divided into two categories; tumors with defined genetic alterations and tumors with various genetic alterations (9) The former group consists of tumors with oncogenic fusion genes created by reciprocal translocations such as the *SYT-SSX* gene in synovial sarcomas (30) and tumors with point mutations in specific genes such as the *KIT* mutation in gastrointestinal stromal tumors (31). In more frequently observed latter group, histological diagnoses varied and a considerable portion of tumors had no specific features and were designated undifferentiated sarcoma (UDSs). Mutations of tumor suppressor genes such as the *RB* and p53 genes were found frequently, but not always (32, 33). Among the 100 tumors analyzed in this study, 28 belonged to the former group and 72 to the latter group.

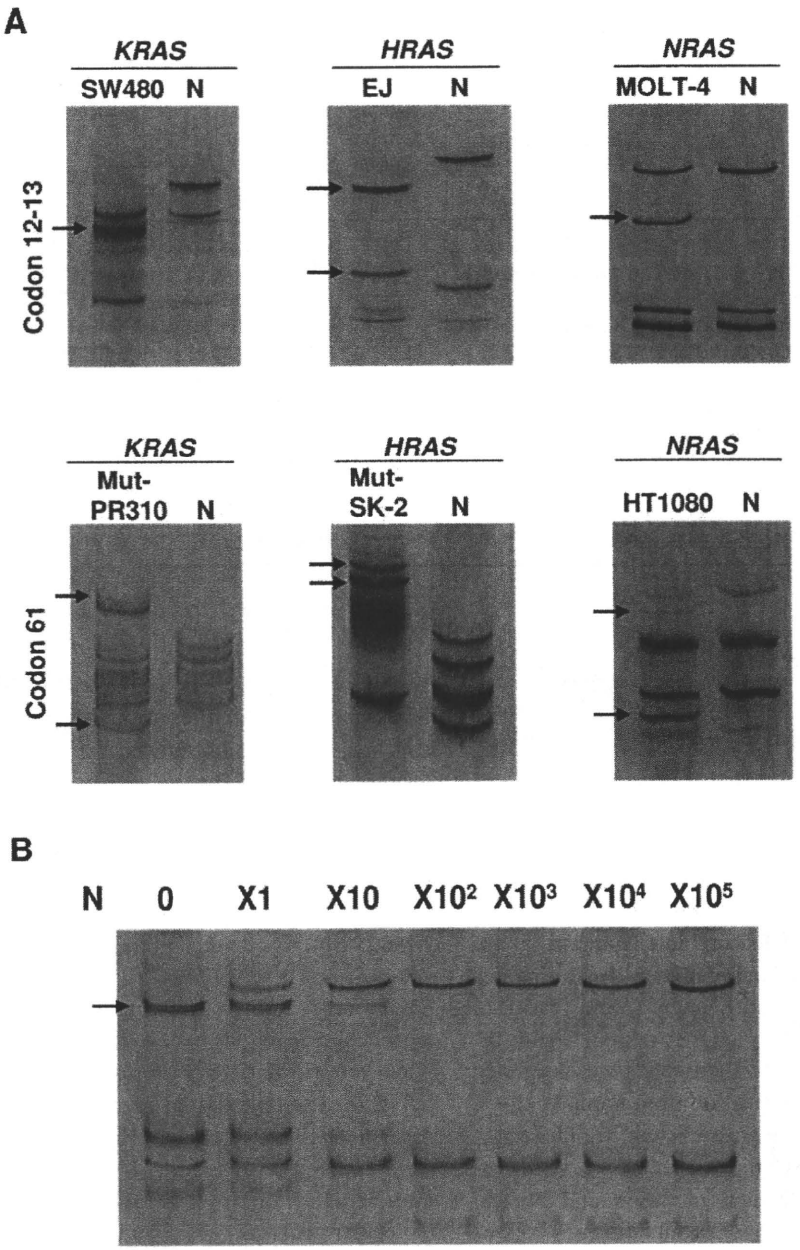

Figure 1. *Detection of mutant fragments by PCR-SSCP. A, Positive controls. PCR fragments encompassing codons 12-13 (upper panel) and codon 61 (lower panel) were amplified using DNA extracted from cell lines or plasmids containing each mutation. Arrows indicate mobility shifted bands. N, Normal skin fibroblast. B, Sensitivity of detection. Normal skin fibroblasts (N) were mixed with EJ cells at the indicated ratio, and DNA extracted from cell mixtures were analyzed by PCR-SSCP using primers for codons 12-13 of the HRAS gene. Arrow indicates mobility shifted bands.*

The detection sensitivity of the PCR-SSCP assay was estimated at 88 to 98% and that of PCR direct sequencing at 97% (34). Despite combining these two methods and using a large number of samples, no mutations were detected in any of three *RAS* genes in the STS samples. The frequencies of *RAS* mutations in STSs varied according to the investigators from 0% to 44% (Table IV). Bohle *et al.* (10) showed that 28% out of 32 malignant fibrous histiocytoma (MFH) samples from German patients contained a point mutation in codon 12 of *HRAS*. However, Rieske *et al.* (12) demonstrated that none out of 35 samples of MFH tissue from patients in Poland contained a point mutation or any other change within or around codons 12 and 13 of the *HRAS* gene. Rieske *et al.* suggested the differences in results could be connected with the ethnic and genetic heterogeneity of the study population. Yoo *et al.* evaluated 45 STS samples from Korean patients

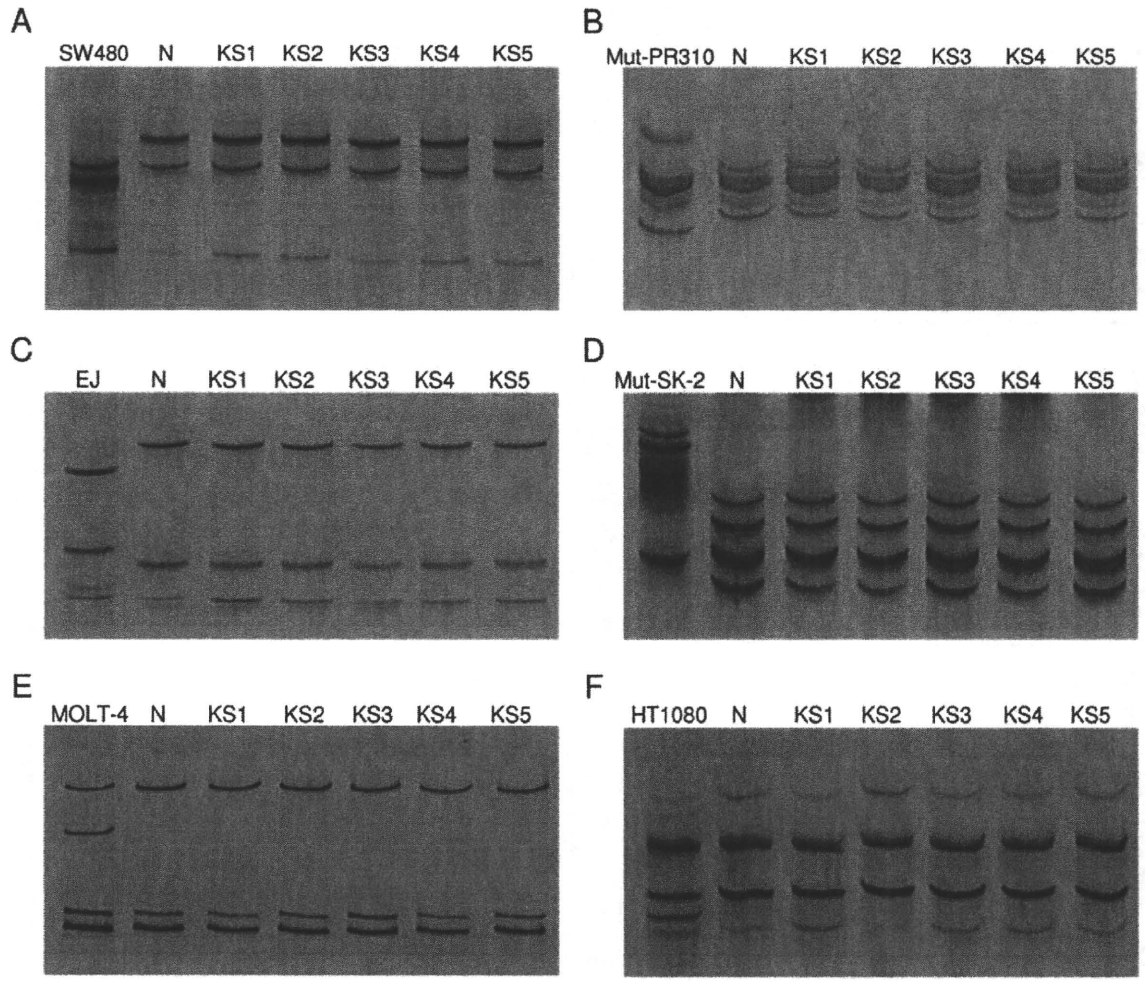

Figure 2. *PCR-SSCP analyses of STS samples. DNA extracted from five STS samples (KS1 to KS5) analyzed by PCR-SSCP along with positive and negative controls of each region are shown. A, codon 12-13 of KRAS; B, codon 61 of KRAS; C, codon 12-13 of HRAS; D, codon 61 of HRAS; E, codon 12-13 of NRAS; F, codon 61 of NRAS. N, normal skin fibroblasts.*

Table IV. *RAS mutations in soft tissue sarcomas.*

Samples			No. of samples with mutations (%)						Methods	Reference
Diagnoses	Country	No.	*KRAS*		*HRAS*		*NRAS*			
			No. of samples with mutations (%)							
STSs	USA	50	0	(0)	1	(2)	–	–	PCR Direct sequencing	14
Leiomyosarcoma	USA	51	7	(14)	–	–	–	–	DGGE	10
Embryonal RMS	UK	14	2	(14)	0	(0)	3	(21)	Probe hybridization	9
MFH	Germany	32	–	–	9	(28)	–	–	PCR Direct sequencing	10
MFH	Poland	35	–	–	0	(0)	–	–	PCR-RFLP & Direct sequencing	12
STSs	Sweden	3	–	–	0	(0)	–	–	Probe hybridization	16
STSs	Korea	45	20	(44)	7	(16)	–	–	Direct sequencing	13
Synovial sarcoma	Japan	49	–	–	3	(6)	–	–	PCR-RFLP	15
RMS	Japan	29	–	–	0	(0)	–	–	PCR-RFLP	17
STSs	Japan	100	0	(0)	0	(0)	0	(0)	PCR-SSCP & Direct sequencing	This study

STSs, Soft tissue sarcomas; RMS: rhabdomyosarcoma; MFH: malignant fibrous histiocytoma; DGGE: denaturing gradient gel electrophoresis; PCR-RFLP: PCR restriction fragment length polymorphism; –, not examined.

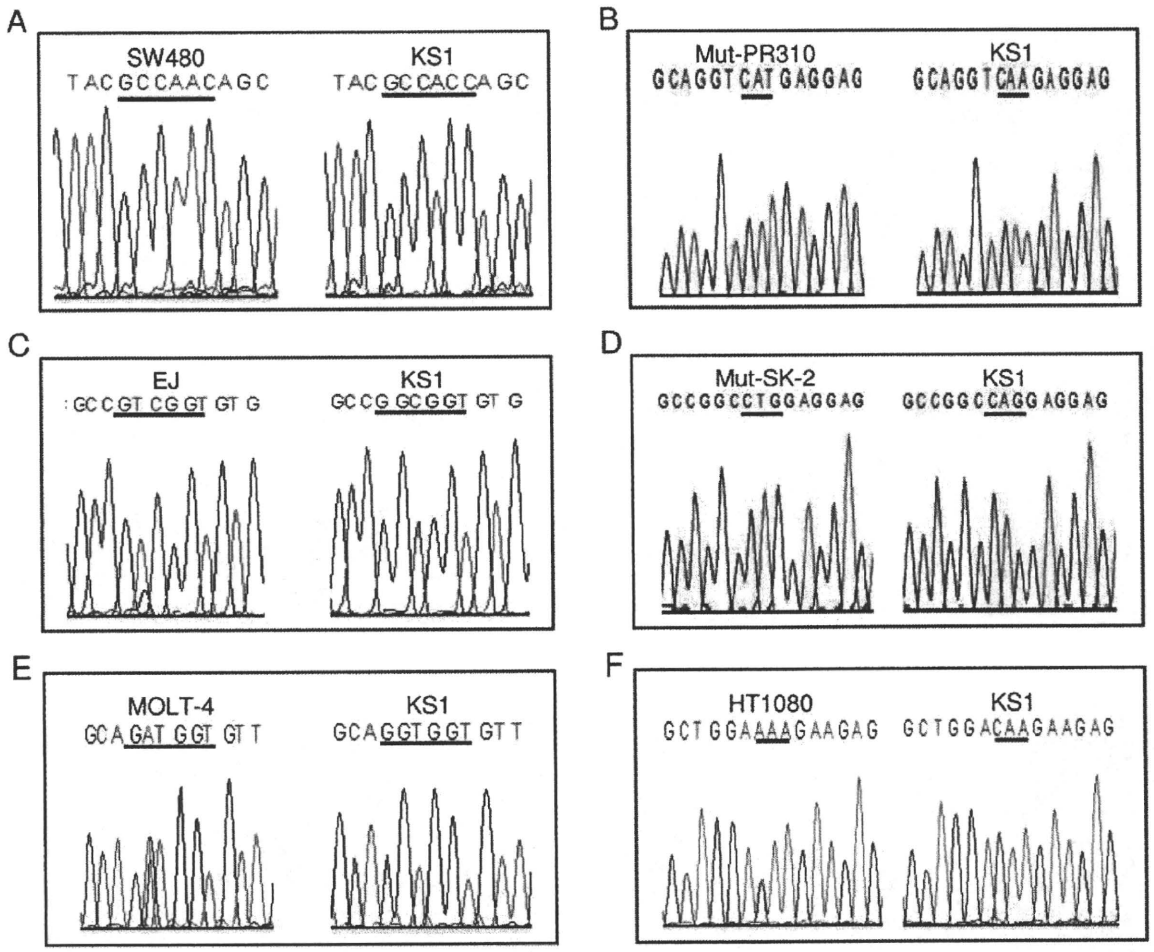

Figure 3. *Direct sequencing analyses of RAS genes. Sequencing data for the positive control and one STS sample (KS1) are shown. Sequences of target regions are underlined. A, codon 12-13 of KRAS; B, codon 61 of KRAS; C, codon 12-13 of HRAS; D, codon 61 of HRAS; E, codon 12-13 of NRAS; F, codon 61 of NRAS. All sequence data were obtained with forward primers except A, which was obtained with a reverse primer.*

and detected *KRAS* and *HRAS* mutations in 44% and 16%, respectively (13). Interestingly, they detected only 1 (2%) mutation at codon 12 of *HRAS* in 50 STS samples from American patients using the same analytical procedures (14), suggesting that genetic and/or environmental factors may affect the occurrence of *RAS* mutations. This might be one of the reasons for our failure to detect *RAS* mutations in the STS samples from Japanese patients. Evidence supporting the above assumption can be found in different types of carcinomas (35, 36). The low frequency of STSs with *RAS* gene mutations may raise concern about the use of HT1080 as a representative cell line of STS.

In conclusion, activated *RAS* mutations are uncommon in STSs samples from Japanese patients and considering the important oncogenic function of Ras-mediated signals, molecular mechanisms compensating for the role of mutated *RAS* may exist in STSs, which could be candidates for targeting of molecular therapy.

Conflict of Interest

None to be declared.

Acknowledgements

We thank Dr. Y. Nakashima for pathological consultations. This work was supported by Grants-in-aid for Scientific Research from the Japan Society for the Promotion of Science, from the Ministry of Education, Culture, Sports, Science and Technology and from the New Energy and Industrial Technology Development Organization.

References

1 Barbacid M: Ras genes. Annu Rev Biochem *56*: 779-827, 1987.
2 Bos JL: The ras gene family and human carcinogenesis. Mutat Res *195*: 255-271, 1988.
3 Land H, Parada LF and Weinberg RA: Tumorigenic conversion of primary embryo fibroblasts requires at least two cooperating oncogenes. Nature *304*: 596-602, 1983.

4 Yancopoulos GD, Nisen PD, Tesfaye A, Kohl NE, Goldfarb MP and Alt FW: N-myc can cooperate with ras to transform normal cells in culture. Proc Natl Acad Sci USA *82*: 5455-5459, 1985.
5 Shima Y, Okamoto T, Aoyama T, Yasura K, Ishibe T, Nishijo K, Shibata KR, Kohno Y, Fukiage K, Otsuka S, Uejima D, Nakayama T, Nakamura T, Kiyono T and Toguchida J: *In vitro* transformation of mesenchymal stem cells by oncogenic H-rasVal12. Biochem Biophys Res Commun *353*: 60-66, 2007.
6 Bos JL: Ras oncogenes in human cancer: a review. Cancer Res 49: 4682-4689, 1989.
7 Cooper CS and Stratton MR: Soft tissue tumours: the genetic basis of development. Carcinogenesis *12*: 155-165, 1991.
8 Enzinger FM and Weiss SW: Soft Tissue Tumors, Third ed., Mosby, St.Louis, MO, 1995.
9 Stratton MR, Fisher C, Gusterson BA and Cooper CS: Detection of point mutations in N-ras and K-ras genes of human embryonal rhabdomyosarcomas using oligonucleotide probes and the polymerase chain reaction. Cancer Res *49*: 6324-6327, 1989.
10 Bohle RM, Brettreich S, Repp R, Borkhardt A, Kosmehl H and Altmannsberger HM: Single somatic ras gene point mutation in soft tissue malignant fibrous histiocytomas. Am J Pathol *148*: 731-738, 1996.
11 Hill MA, Gong C, Casey TJ, Menon AG, Mera R, Gillespie AT, Giardina JF, Levine EA and Hunt JD: Detection of K-ras mutations in resected primary leiomyosarcoma. Cancer Epidemiol Biomarkers Prev *6*: 1095-1100, 1997.
12 Rieske P, Bartkowiak J, Szadowska A and Debiec-Rychter M: Malignant fibrous histiocytomas and H-ras-1 oncogene point mutations. Mol Pathol *52*: 64-67, 1999.
13 Yoo J, Robinson RA and Lee JY: H-ras and K-ras gene mutations in primary human soft tissue sarcoma: concomitant mutations of the ras genes. Mod Pathol *12*: 775-780, 1999.
14 Yoo J and Robinson RA: H-ras and K-ras mutations in soft tissue sarcoma: comparative studies of sarcomas from Korean and American patients. Cancer *86*: 58-63, 1999.
15 Oda Y, Sakamoto A, Satio T, Kawauchi S, Iwamoto Y and Tsuneyoshi M: Molecular abnormalities of p53, MDM2, and H-ras in synovial sarcoma. Mod Pathol *13*: 994-1004, 2000.
16 Barrios C, Castresana JS, Ruiz J and Kreicbergs A: Amplification of the c-myc proto-oncogene in soft tissue sarcomas. Oncology *51*: 13-17, 1994.
17 Takahashi Y, Oda Y, Kawaguchi K, Tamiya S, Yamamoto H, Suita S and Tsuneyoshi M: Altered expression and molecular abnormalities of cell-cycle-regulatory proteins in rhabdomyosarcoma. Mod Pathol *17*: 660-669, 2004.
18 Ishibe T, Nakayama T, Okamoto T, Aoyama T, Nishijo K, Shibata KR, Shima Y, Nagayama S, Katagiri T, Nakamura Y, Nakamura T and Toguchida J: Disruption of fibroblast growth factor signal pathway inhibits the growth of synovial sarcomas: potential application of signal inhibitors to molecular target therapy. Clin Cancer Res *11*: 2702-2712, 2005.
19 Sonobe H, Manabe Y, Furihata M, Iwata J, Oka T, Ohtsuki Y, Mizobuchi H, Yamamoto H, Kumano O and Abe S: Establishment and characterization of a new human synovial sarcoma cell line, HS-SY-II. Lab Invest *67*: 498-505, 1992.
20 Kawai A, Naito N, Yoshida A, Morimoto Y, Ouchida M, Shimizu K and Beppu Y: Establishment and characterization of a biphasic synovial sarcoma cell line, SYO-1. Cancer Lett *204*: 105-113, 2004.
21 Nojima T, Wang YS, Abe S, Matsuno T, Yamawaki S and Nagashima K: Morphological and cytogenetic studies of a human synovial sarcoma xenotransplanted into nude mice. Acta Pathol Jpn *40*: 486-493, 1990.
22 Imaizumi S, Motoyama T, Ogose A, Hotta T and Takahashi HE: Characterization and chemosensitivity of two human malignant peripheral nerve sheath tumour cell lines derived from a patient with neurofibromatosis type 1. Virchows Arch *433*: 435-441, 1998.
23 Hosoi H, Sugimoto T, Hayashi Y, Inaba T, Horii Y, Morioka H, Fushiki S, Hamazaki M and Sawada T: Differential expression of myogenic regulatory genes, MyoD1 and myogenin, in human rhabdomyosarcoma sublines. Int J Cancer *50*: 977-983, 1992.
24 Sambrook J, Molecular Cloning: A Laboratory Manual (Third ed.). Cold Spring Harbor Laboratory Press, Cold Spring Harbor, NY, 2001.
25 Suzuki Y, Orita M, Shiraishi M, Hayashi K and Sekiya T: Detection of ras gene mutations in human lung cancers by single-strand conformation polymorphism analysis of polymerase chain reaction products. Oncogene *5*: 1037-1043, 1990.
26 Orita M, Suzuki Y, Sekiya T and Hayashi K: Rapid and sensitive detection of point mutations and DNA polymorphisms using the polymerase chain reaction. Genomics *5*: 874-879, 1989.
27 Aoyama T, Nagayama S, Okamoto T, Hosaka T, Nakamata T, Nishijo K, Tsuboyama T, Nakayama T, Nakamura T and Toguchida J: Mutation analyses of the NFAT1 gene in chondrosarcomas and enchondromas. Cancer Lett *186*: 49-57, 2002.
28 Hayashi K: PCR-SSCP: a simple and sensitive method for detection of mutations in the genomic DNA. PCR Methods Appl *1*: 34-38, 1991.
29 Toguchida J and Nakayama T: Molecular genetics of sarcomas: Applications to diagnoses and therapy. Cancer Sci *100*: 1573-1580, 2009.
30 Ladanyi M: Fusions of the SYT and SSX genes in synovial sarcoma. Oncogene *20*: 5755-5762, 2001.
31 Fletcher JA and Rubin BP: KIT mutations in GIST. Curr Opin Genet Dev *17*: 3-7, 2007.
32 Sabah M, Cummins R, Leader M and Kay E: Aberrant expression of the Rb pathway proteins in soft tissue sarcomas. Appl Immunohistochem Mol Morphol *14*: 397-403, 2006.
33 Taubert, H Meye A and Wurl P: Soft tissue sarcomas and p53 mutations. Mol Med *4*: 365-372, 1998.
34 Hestekin CN and Barron AE: The potential of electrophoretic mobility shift assays for clinical mutation detection. Electrophoresis *27*: 3805-3815, 2006.
35 Scarpa A, Capelli P, Villaneuva A, Zamboni G, Lluis F, Accolla R, Mariuzzi G and Capella G: Pancreatic cancer in Europe: Ki-ras gene mutation pattern shows geographical differences. Int J Cancer *57*: 167-171, 1994.
36 Konishi N, Hiasa Y, Tsuzuki T, Tao M, Enomoto T and Miller GJ: Comparison of ras activation in prostate carcinoma in Japanese and American men. Prostate *30*: 53-57, 1997.

Received August 18, 2009
Revised December 8, 2009
Accepted December 9, 2009

Biochemical and Biophysical Research Communications 391 (2010) 1471–1476

Contents lists available at ScienceDirect

Biochemical and Biophysical Research Communications

journal homepage: www.elsevier.com/locate/ybbrc

Mesenchymal stem cells cultured under hypoxia escape from senescence *via* down-regulation of p16 and extracellular signal regulated kinase

Yonghui Jin [a], Tomohisa Kato [a], Moritoshi Furu [a], Akira Nasu [a,b], Yoichiro Kajita [a,c], Hiroto Mitsui [a,d], Michiko Ueda [a], Tomoki Aoyama [e], Tomitaka Nakayama [b], Takashi Nakamura [b], Junya Toguchida [a,b,f,*]

[a] *Department of Tissue Regeneration, Institute for Frontier Medical Sciences, Kyoto University, Japan*
[b] *Department of Orthopaedic Surgery, Graduate School of Medicine, Kyoto University, Japan*
[c] *Department of Urology, Graduate School of Medicine, Kyoto University, Japan*
[d] *Department of Musculoskeletal Medicine, Graduate School of Medical Sciences, Nagoya City University, Japan*
[e] *Human Health Sciences, Graduate School of Medicine, Kyoto University, Japan*
[f] *Center for iPS Cell Research and Application, Institute for Integrated Cell – Material Sciences, Kyoto University, Japan*

ARTICLE INFO

Article history:
Received 12 December 2009
Available online 23 December 2009

Keywords:
Mesenchymal stem cell
Hypoxia
Senescence
p16
Extracellular signal regulated kinase

ABSTRACT

Hypoxia has been considered to affect the properties of tissue stem cells including mesenchymal stem cells (MSCs). Effects of long periods of exposure to hypoxia on human MSCs, however, have not been clearly demonstrated. MSCs cultured under normoxic conditions (20% pO_2) ceased to proliferate after 15–25 population doublings, while MSCs cultured under hypoxic conditions (1% pO_2) retained the ability to proliferate with an additional 8–20 population doublings. Most of the MSCs cultured under normoxic conditions were in a senescent state after 100 days, while few senescent cells were found in the hypoxic culture, which was associated with a down-regulation of *p16* gene expression. MSCs cultured for 100 days under hypoxic conditions were superior to those cultured under normoxic conditions in the ability to differentiate into the chondro- and adipogenic, but not osteogenic, lineage. Among the molecules related to mitogen-activated protein kinase (MAPK) signaling pathways, extracellular signal regulated kinase (ERK) was significantly down-regulated by hypoxia, which helped to inhibit the up-regulation of *p16* gene expression. Therefore, the hypoxic culture retained MSCs in an undifferentiated and senescence-free state through the down-regulation of p16 and ERK.

Introduction

Mesenchymal stem cells (MSCs) are tissue stem cells with multi-directional differentiation potential, though molecular and cellular definitions remain controversial. At present, MSCs are defined as mononuclear adherent cells capable of differentiating into the osteo-, chondro-, and adipogenic lineages [1]. Despite the equivocal definition, the clinical application of MSCs to tissue regeneration and engineering has already been launched [2,3]. Like other tissue stem cells, MSCs have limited growth potential and cease to proliferate due to cellular senescence [4]. Cellular senescence is induced by both intrinsic and extrinsic factors [5]. The shortening of telomeres is the most important intrinsic factor, and mitogenic stimuli and DNA damage are main extrinsic factors. Oxidative stress caused by reactive oxygen species (ROS) is one of the factors inducing DNA damage [6]. Although cells with the properties of MSCs have been isolated from adipose tissue [7], synovial tissue [8], and umbilical cord [9], bone marrow is the most frequent source of MSCs [10]. The oxygen concentration (pO_2) in bone marrow varies by the distance from the sinus ranging from 1% to 7% [11]. Therefore, although the precise location of MSCs in bone marrow is not known, the physiological oxygen concentration surrounding MSCs is much lower than the ambient oxygen concentration in cultures (20% pO_2). The high concentration of oxygen in standard culturing systems may produce excess oxidative stress, driving MSCs into a senescent state. Based on this concept, a number of studies have cultured MSCs under hypoxic conditions [12–17], and demonstrated that hypoxia is beneficial to the growth and also differentiation of MSCs, although the precise molecular mechanisms responsible for these phenotypic changes are not clear. The expression of the *p16* tumor suppressor gene is also important to cellular senescence [18,19]. We have shown that *p16* gene expression was gradually up-regulated during the life of MSCs *in vitro*, and tightly associated with the induction of cellular senescence [20]. Inhibition of *p16* gene expression by short interfering RNA for *p16* endowed senescent MSCs with the ability to re-proliferate and rescued them from senescence, indicating

* Corresponding author. Address: Institute for Frontier Medical Sciences, Kyoto University, 53 Kawahara-cho, Shogoin, Sakyo-ku, Kyoto 606-8507, Japan. Fax: +81 75 751 4646.
E-mail address: togjun@frontier.kyoto-u.ac.jp (J. Toguchida).

0006-291X/$ - see front matter © 2010 Published by Elsevier Inc.
doi:10.1016/j.bbrc.2009.12.096

the important role of p16 in the growth of MSCs [20]. A number of factors are involved in the up-regulation of *p16* gene expression *in vitro* including ROS [21].

Here we cultured MSCs long term (more than 200 days) under normoxic (20% pO_2) or hypoxic (1% pO_2) conditions, and compared growth profiles and the potential to differentiate into three lineages. We found that hypoxia increased the life span of MSCs by down-regulating *p16* gene expression and endowed superior properties for differentiation into the chondro-, and adipogenic lineages, which were associated with the down-regulation of extracellular signal regulated kinase (ERK).

Materials and methods

Primary cultured cells

The isolation of bone marrow-derived MSCs from donors was performed as described previously [22]. The Ethics Committee of the Faculty of Medicine, Kyoto University, approved the procedure and informed consent was obtained from each donor. Mononuclear cells containing MSCs were suspended in α-minimal essential medium with GlutaMAX (Invitrogen Co., Carlsbad, CA) supplemented with 10% fetal bovine serum (HyClone, South Logan, UT), 100 U/ml penicillin, and 100 mg/ml streptomycin, and separately cultured at a density of 2.5×10^5 cells/cm^2 under normoxic (20% pO_2 and 5% pCO_2) and hypoxic (1% pO_2 and 5% pCO_2) conditions at 37 °C. At 80% confluence, cells were collected, counted, and reseeded at a density of 3000 cells/cm^2. From this point, the number of population doublings (PD) was calculated based on the total cell number at each passage.

Senescence-associated-β-galactosidase assay

Cells were cultured on four-well chamber slides. The senescence-associated-β-galactosidase (SA-β-gal) assay was performed with a Senescence Detection Kit (BioVison, Mountain View, CA).

Induction of differentiation and quantitative evaluation

Differentiation was induced using standard methods [23], and evaluated quantitatively as follows.

Osteogenic differentiation. After 14 days, calcium deposits were visualized by alizarin red staining, and calcium content was quan-

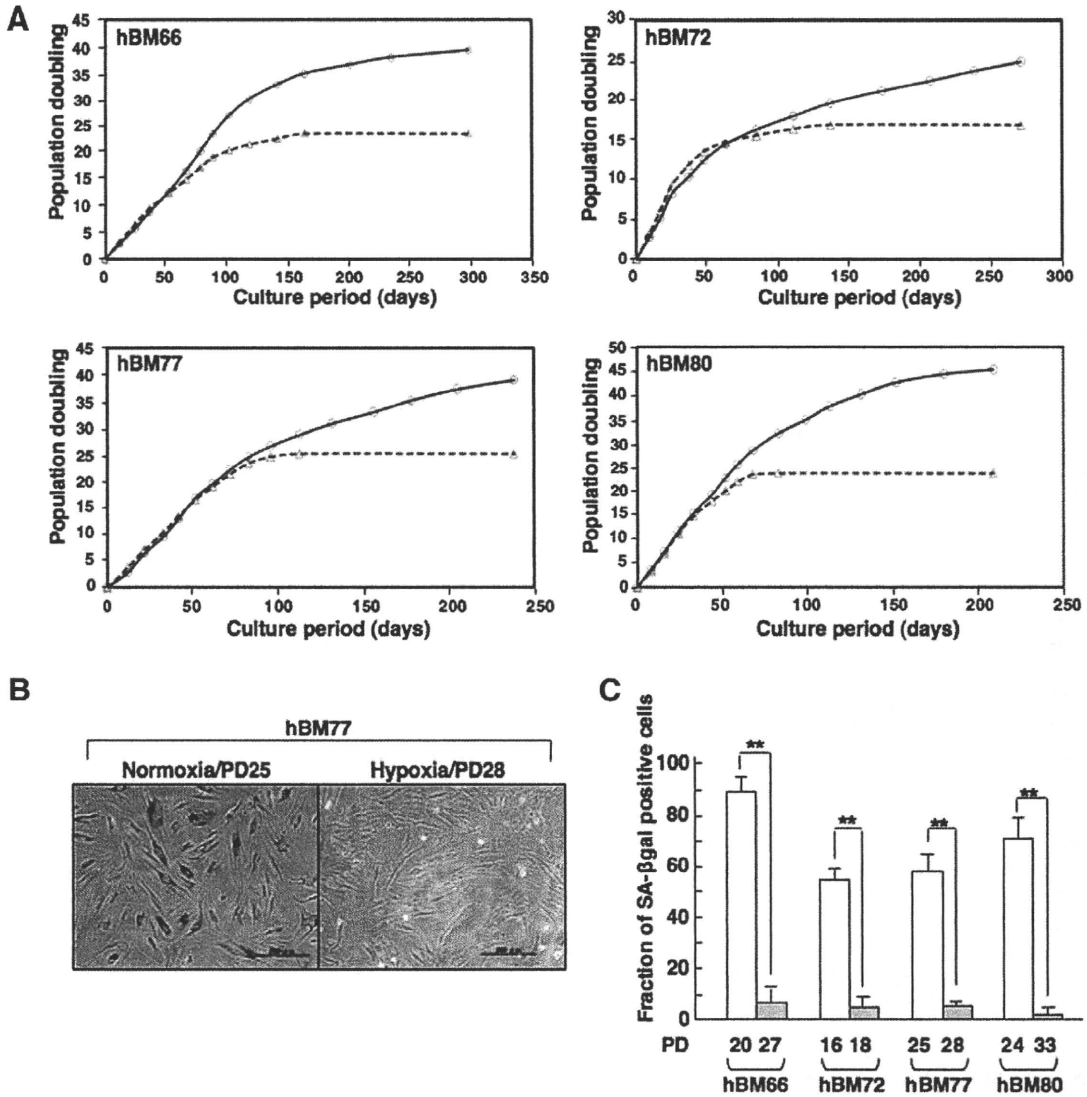

Fig. 1. Hypoxia extended the life span of MSCs *in vitro*. (A) Growth profiles of MSCs under normoxic (blue triangle) and hypoxic (red triangle) conditions. (B) Expression of SA-β-gal. hBM77 cells cultured for about 100 days under normoxic (PD25) or hypoxic (PD28) conditions were stained. (C) Quantitative analyses of SA-β-gal-positive cells among four hBM cell preparations at the indicated PD. White and gray box indicate normoxic and hypoxic conditions, respectively. (For interpretation of the references to color in this figure legend, the reader is referred to the web version of this paper.)

tified based on the OCPC method with a Calcium C-Test Wako Kit (Wako Pure Chemical Industries, Osaka, Japan).

Adipogenic differentiation. After 21 days, lipid-vacuoles were detected using Oil-Red-O staining, and the amount of triglyceride (TG) was quantified with a serum triglyceride kit (Sigma–Aldrich, St. Louis, MO). Protein content was quantified using BCA protein assay reagent (Pierce Biotechnology, Rockford, IL).

Chondrogenic differentiation. After 14 days, cartilage matrix was evaluated by alcian blue staining of cryosections, and the glycosaminoglycan (GAG) content in pellets was quantified with BLYSCAN Dye and Dissociation reagents (BIOCOLOR, Belfast, UK). DNA content was quantified using a PicoGreen dsDNA Quantitation kit (Invitrogen, Carlsbad, CA).

Western blotting

Western blotting was performed as described [22]. The primary antibodies used were as follows: MAB1536 for HIF-1α, purchased from R&D Systems (Minneapolis, MN), and 551153 for p16, M12320 for ERK1, E23920 for phosphorylated ERK1/2, P19820 for p38, P39520 for phosphorylated p38, M54920 for pan-JNK, and S37220 for phosphorylated JNK, purchased from BD Biosciences Pharmingen (San Diego, CA). Blots were probed with horseradish peroxidase-conjugated goat anti-mouse IgG or goat anti-rabbit IgG (Santa Cruz Biotechnology, Santa Cruz, CA) and visualized using a chemiluminescence reagent ECL Plus Detection Kit (GE Healthcare UK Ltd., Little Chalfont, UK). The intensity of each band was calculated with Quantity One software, and evaluated as a ratio to that of control (β-actin).

Cell treatment

MAPK/ERK kinase (MEK) inhibitor treatment. Cells (2×10^5) were treated with U0126 (10 μM) (Promega, Madison, WI) for 96 h, and proteins were extracted every 24 h for Western blotting.

n-Propyl gallate (nPG) treatment. Cells (8×10^4) were treated with nPG (Sigma–Aldrich) at a concentration of 25–200 μM for 4 h, and proteins were extracted for Western blotting.

Statistical analyses

Statistical analyses were performed using Statcel software. Data were assessed using the Pearson product-moment correlation coefficient and Student's *t*-test.

Results

Hypoxia elongated growth of MSCs

MSCs were isolated from bone marrow of four donors, designated hBM66, hBM72, hBM77, and hBM80, respectively, and cultured under normoxic or hypoxic conditions as described in Materials and methods. In the case of hBM66, there was no significant difference between normoxic and hypoxic cultured-cells in terms of growth profile until PD15 (Fig. 1). After this stage, normoxic cultured-cells ceased to proliferate, whereas hypoxic cultured-cells kept on growing, and the number of PD at the last observation under normoxic and hypoxic conditions was 24 and 40, respectively. The theoretically accumulated cell number was 65,000-fold

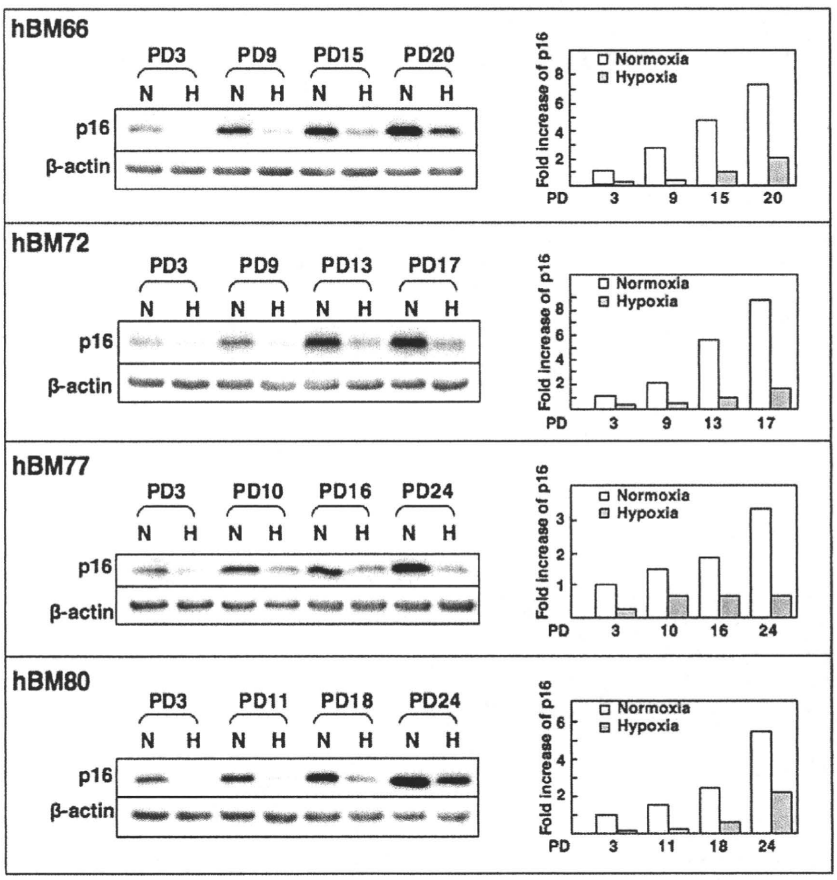

Fig. 2. Hypoxia down-regulated the expression of p16 in MSCs. Expression of p16 was evaluated by Western blotting using antibody for p16 protein. The relative expression level was determined using the value at PD3 of normoxic cultured-cells as a standard. White and gray box indicate normoxic and hypoxic conditions, respectively.